Modeling and Analysis

GREENHOUSE GASES SCIENCE AND TECHNOLOGY

Controlling potential far-field brine leakage from CO_2 storage formations using deep extraction wells: Numerical and experimental testing

Ahmad H. Askar, INTERA Inc. Boulder, Boulder, Colorado, USA
Tissa H. Illangasekare, Center for Experimental Study of Subsurface Environmental Processes, Department of Civil and Environmental Engineering, Colorado School of Mines, Golden, Colorado, USA

Abstract: Injecting CO_2 into deep geologic formations for storage purposes induces large pressure build-up that risks caprock integrity. Naturally occurring faults or pressure-induced fractures in the caprock can act as conductive leakage pathways resulting in potential contamination of the overlying shallow aquifers. Previous studies explored using brine extraction to manage such elevated pressure in the storage formation. In this paper, we extended the use of this technique to control far-field brine leakage. Extraction wells are placed in the storage zone to reduce the leakage flow through reversing the pressure-gradient locally, while minimizing the brine concentrations in the escaped-fraction by utilizing the dilution capacity of the overlying formations. The developed approach incorporated the Genetic Algorithm with transport model simulations to optimize well-placements and extraction-rates. An approximately 8m long intermediate-scale tank designed to mimic brine leakage migration in the field was used to validate this approach as field data are not available. We further evaluated the approach numerically using a hypothetical leakage scenario at the Vedder storage formation in San-Joaquin basin to assess its practicality for field implementation. The results showed that storage zone heterogeneity and fractures' permeabilities can significantly affect the optimum locations and pumping rates of the extraction wells. Brine leakage can be controlled by extracting a native-brine volume less than 50% of the injected CO_2 volume. The target concentrations in the shallow aquifer determines the extraction rates required to control a leakage through a fracture or a buried thrust fault. The study is useful to develop remediation strategies for carbon storage operations. © 2022 Society of Chemical Industry and John Wiley & Sons, Ltd.

Keywords: CO_2 sequestration; brine leakage management; genetic algorithm; intermediate scale testing

Correspondence
Ahmad Askar, INTERA Inc. Boulder, CO, USA.
Email: ahmedaskar6@gmail.com
Received August 31, 2022; revised November 30, 2022; accepted December 1, 2022
Published online at Wiley Online Library (wileyonlinelibrary.com). DOI: 10.1002/ghg.2194

Introduction

Geologic carbon storage (GCS) into deep saline formations is a promising technology applied for minimizing the amount of released CO_2 to the atmosphere contributing to global warming.[1–4] The pressure build-up in the storage formation during CO_2 injection can affect the caprock integrity, which can lead to pressure-driven leakage of native brine or CO_2, posing a contamination risk on the underground sources of drinking water (USDWs). This leakage can occur via existing or pressure-induced conductive pathways, such as activated faults, caprock fractures, abandoned wells, and opened cracks/fissures.[5–8] The pressure increase in the storage formation can reach far distances from the injection site due to the rapid propagation of the pressure waves,[9] which makes investigating the potential leakage pathways complex and costly.[10]

In order to reduce the potential geomechanical risks of the storage zone pressure build-up on far-field caprock integrity (e.g., induced seismicity, fault activation, and fracture opening), different studies proposed brine extraction as an efficient pressure management technique.[11–14] Brine extraction can also increase the available CO_2 storage capacity, limit the area of site characterization and risk assessment, decouple neighboring GCS operations by minimizing the pressure overlap areas, and enhance CO_2 trapping efficiency.[13,15–17] Extracted brine can be used as a feedstock for both desalination plants and cooling/heating facilities or can be reinjected in different over- or underlying saline formations for disposal purposes.[13,17]

In recognition of the high cost of brine handling process,[18] Birkholzer et al.[12] and Cihan et al.[19] explored different design approaches to minimize the extraction volume of brine while maintaining the controlled pressure at stressed faults in the storage zone below critical values. To extract the smallest possible volume of brine, they treated the locations and extraction rates of the wells as variables in an optimization framework. Lately, González-Nicolás et al.[20] emphasized that the results of such optimization can be biased due to the lack of accurate information about the subsurface geological settings, which can lead to poor design of the extraction system and thus elevated pressure in the storage zone. This uncontrolled pressure build-up may cause different modes of failures in the caprock, including fault activation, fracture opening, dilating, and intersecting with other damage zones,[21,22] which will pose a high leakage risk on the USDWs.

Based on above, it can be argued that designing the extraction system to control the potential brine leakage from storage formations instead of just managing the pressure build-up (that was addressed by a number of previous studies) can be more critical to environmental safety of GCS operations[23] and need to be evaluated. Particularly that developing a remedial response strategy for GCS projects is one of the EPA recommendations.[24] Therefore, the concept of designing the extraction wells to control the post-caprock-failure brine leakage, and not only managing the pre-caprock-failure repository pressure, is crucial for the evaluation and validation on various scales and under different uncertainty scenarios as a step forward for field implementation, which is the main objective of this study. Conceptually, far-field brine leakage will be controlled through reversing a significant portion of the advective leakage flux back to the storage zone by extraction and utilizing the overlying groundwater regimes to dilute the escaping fraction of the leaking mass. A design approach of such system should include finding the optimal well locations that provide the lowest extraction rates to control the leakage and constrain the brine concentrations in the shallow aquifer to be less than either the maximum contaminant level (MCL) set by EPA[25] or the site-specific no-impact threshold value (NITV)[26] depending on state regulations and project's permit. Notably, many researchers emphasized the importance of using NITVs instead of MCLs to evaluate the impact of CO_2 and brine leakage on the shallow aquifers due to the continuous change of groundwater chemistry with time.[27–35]

The question that might be raised here is "can such a leakage control system be utilized to manage the pressure build-up in the storage reservoir prior to the onset of any leakage events?" To answer this question, it is necessary to point out that locating pressure-relief wells in the storage zone is relatively more flexible than locating leakage-control wells. This is due to the drastic difference between the propagation velocities of a pressure signal and a leakage plume in the subsurface environments.[13,17] Hence, reservoir pressure can be managed by leakage control wells located far away from the injection site until a leakage event happens. It should be noted that such operational conditions will also allow for satisfying the EPA requirement of developing the extraction system as an emergency

response tool that is actively operated when a leakage event occurs.[24]

Several simulation-based optimization approaches have been reported in the literature for several types of groundwater problems.[36,37] In the context of GCS management, Birkholzer et al.[12] applied a derivative-based method to find the optimum extraction scheme to control the reservoir pressure. Cihan et al.,[19] argued that the irregularity of the objective function in the optimal well placement problems can lead to suboptimal solutions if derivative-based methods were employed. Therefore, Cihan et al.[19] and González-Nicolás et al.[20] relied on using the global optimizer of differential evolution to find the best locations and rates of the pressure relief wells. Cameron and Durlofsky[16] employed the pattern search optimizer of Hooke-Jeeves to place the injection and production wells in optimal locations that enhance the brine cycling process needed for minimizing the mobile fraction of CO_2 in the storage formation. Zhang and Agarwal[38] and Liu et al.[39] incorporated the genetic algorithm (GA) with the multiphase simulator TOUGH240 to optimize the injection pressure, rate, and depth to reach the maximum CO_2 storage capacity with minimum adverse environmental impacts. Recently, Liu et al.[41] used the GA to optimize the pumping rate and well placement of one CO_2 injection well and four production wells to enhance the GCS operation in a CO_2 enhanced gas recovery site. In other applications, the GA was also successfully used for well placement optimization problems related to oil and gas development.[42–44]

Study approach brief

A design approach that incorporates the global optimizer GA with FEFLOW-based transport model[45] was used in this study to find the best extraction well locations in the CO_2-storage formation to control potential far-field brine leakage. It is reasonable to assume that field testing and validation of such a design approach is not technically and financially feasible. At the same time, relying solely on numerical modeling tools to test this approach can make the study findings questionable due to the inherent uncertainty in model predictions of brine migration resulting from errors in model structure and parameters.[46] Thus, a validation approach that combines respectively intermediate- and full-scale experimental and numerical testing was used in this study to evlauate the proposed design method. The intermediate-scale laboratory data were used to examine the applicability of using the developed design approach under moderate uncertainty conditions (some data about the deep geological settings are available) similar to what are expected in the intensively investigated GCS sites during oil exploration campaigns. In addition, a stochastic assessment was conducted to evaluate the suitability of using the proposed design approach under extreme uncertainty conditions (sparse and inaccurate date about the deep geological settings are available) that are expected in the unexplored GCS sites for the purpose of oil production. This was followed by a hypothetical field-scale study using the flow and transport simulator FEFLOW to evaluate the brine extraction practicality as a control tool under field-relevant leakage scenarios.

The validation experiment was conducted in an approximately 8m soil tank presented in Askar et al.[47] In this tank, the migrating far-field brine from the storage formation to the shallow aquifer was controlled by an extraction system designed based on the GA optimization analysis. The validity of the approach was tested by evaluating whether the observed plume concentrations in the shallow aquifer met the predefined constraining limits in the optimization problem. For the numerical testing, a hypothetical leakage plume generated from the Pond fault at the Vedder formation in San Joaquin Basin in California was simulated. The Vedder formation is a potential CO_2 storage reservoir with a target injection rate of 5 MT CO_2/year for a period of 50 years.[48–50] In this analysis, an extraction well was selected and operated based on the GA results to control the simulated leakage. Then, the ratio between the required brine-volume to be extracted to control the leakage and the planned CO_2-volume to be injected was used as a practicality indicator following Birkholzer et al.,[12] Cihan et al.,[19] and González-Nicolás et al.[20]

Optimization approach

The GA modified by Deep et al.,[51] and rooted in the global optimization toolbox in MATLAB 2019b[52] was used. The simulation-based optimization relies on running the forward model many times until the global minimum of an objective function that meets a set of constraints is found. The optimization problem entails finding the best locations and pumping rates of the extraction wells that can control the potential leakage from a CO_2 storage zone by extracting the minimum

amount of the formation brine. The objective function, including problem constraints, used for this analysis can be expressed as:

$$\min_{u\in\Omega} J(u)\,, \text{ subject to } \rightarrow w.\,[C(u) \le C_T]\,, \qquad (1)$$

where J is the objective function to be minimized representing the total pumping rate from all selected wells, and u is a matrix of the optimization variables including well locations (W) and pumping rates ($\mathbf{Q}$), where Ω refers to the variable bounds. C is a vector of the simulated leakage concentrations at specific locations in the shallow aquifer that is subjected to a vector of weighted constraints representing the plume target concentrations (C_T) at same locations. C_T can be defined based on either the MCLs or NITVs depending on the regulators' decision. Notably in Eqn 1, the weights used with the concentration constraints (w) give the flexibility to prioritize specific zones in the shallow aquifer over others. For example, areas close to drinking water supplies should be given higher weights to meet the concentration constraints. This option is vital for distinguishing between the potable and nonpotable shallow groundwater resources in designing the control system.

To limit the size of the solution space, we assumed that all the locations of the potential extraction wells can be predefined in the model domain. We considered this assumption practical because one cannot place a deep well at any location across the storage zone due to potential technical and regulatory constraints. In addition, the reduced size of the solution space will minimize the computational burden of the optimization process. This assumption makes the selection pool of the GA consist of only positive integers representing the well IDs (e.g., natural numbers), where every well ID corresponds to a certain well location. In contrast, the pumping rates were treated as noninteger positive variables to find the lowest possible pumping rates. Moreover, a nonlinear constraint of the brine plume concentrations at the shallow aquifer was added to the optimization problem. Such constraint was enforced by considering any suggested solution by the GA that violates the predefined concentration limits infeasible through penalizing it in the objective function. For more details on the adapted penalty function, the reader is referred to Deb.[53] Finally, similar to Cihan et al.,[19] the costs of extraction, handling, and treatment of brine were assumed to be proportional to the total pumping rates of the extraction system.

Component C in Fig. 1 presented in Askar et al.[54] shows the general key steps of GA procedure adapted in this study as well to perturb u and find the global minimum of Eqn 1, while satisfying the assigned constraints. The first population matrix (P_1) of the proposed solutions (u_v) generated by the GA has a dimension of $v\times k$, where v is the population size ($v =$ 50 in this study) and k is the number of variables. Notably, $k = 2$ means one extraction well is desired, as each well is defined by one location and one pumping rate. The variables W and Q, composing the u matrix, are randomly sampled by the GA within the defined bounds (Ω) for these variables to construct the P_1. The proposed solutions (u_v) are ranked based on the value of the objective function $J(u_v)$, which is basically a penalty function that can distinguish between feasible and infeasible solutions.[53] Ranked solutions are then processed via the standard producing function of the GA to construct the next population matrix (P_1). The assumptions used for setting up the GA in this study are as follows: 40% of the prior population is maintained in the next population as elite candidates, the two top-ranked candidates are treated as parents to produce 15% of the offspring using Laplace crossover function, while the rest of the offspring is produced using a Power mutation function.[51] Every time the GA is intended to generate a new population matrix, the ranks of the two previous population candidates are compared to select the elite candidates and parents of the new population matrix. The GA keeps on looping until one of the defined stopping criteria is met; either the resulted optimum values are almost the same over the last 20 trials or the number of generated populations reaches the maximum defined limit (500 in this study).

It is worth mentioning that testing NSGA-II based optimization algorithms, like PESTPP-MOU[55] or the constrained multiobjective Bayesian optimization method[56] for the same problem or more complex cases can give us important insights about the best optimization approach for such problems in terms of accuracy and performance.

Experimental analysis

The developed optimization method was validated using a laboratory test system where a far-field brine leakage event was simulated. This validation analysis

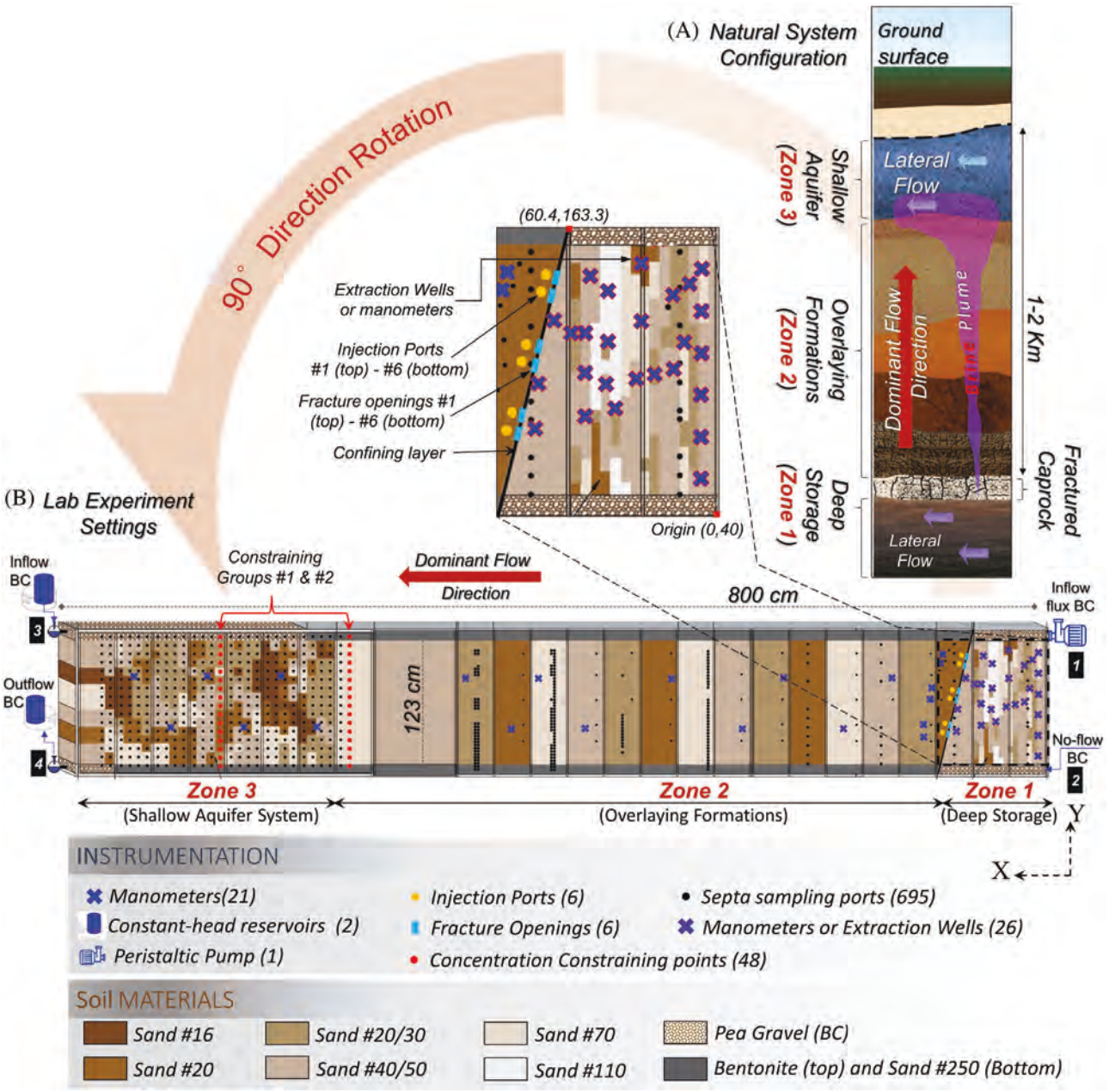

Figure 1. Schematic depicting (A) brine leakage migration from a CO_2 storage formation under natural settings, (B) experimental setup including packing heterogeneity, tank instrumentation and the potential locations of extraction wells. The figure was modified after Askar et al.[47] to show the locations of the placed extraction wells in Zone 1 and the constraining points in Zone 3. Note the flow occurs from right to left.

included the following steps: (1) placing dozens of extraction wells in the storage reservoir of the test tank for the GA selection, (2) conducting multiple transport simulations for different possible leakage scenarios to generate an extended solution space so that the most optimal control system is selected by the GA under moderate uncertainty conditions, (3) implementing the extraction scheme in the test tank and evaluate its performance by checking whether the controlled plume violated the constraining concentrations in the shallow aquifer, (4) appraising the degree of optimality of the GA results by quantifying the impact of minor deviations in the optimal solution on the control-system efficacy using numerical tools, (5)

assessing the sensitivity of the optimization results towards the variability in the system parameters, and (6) finally, evaluating the suitability of using the proposed design approach in a stochastic framework to handle sites with extreme uncertain data about the system.

The proceeding subsections start by a brief description of the laboratory test system and the formulated optimization problem to design the far-field brine leakage control wells in the tank. Thereafter, the results of the experimental validation, optimality check, and sensitivity analysis are presented and discussed.

Soil tank experimental setup

Several challenges need to be overcome to simulate an upward far-field brine leakage in a laboratory testing system with the existing physical space constrains. These challenges include: (1) the large depths of the geological formations associated with the leakage problem, (2) the expected complex geological settings, and (3) the multidimensional flow fields controlling the leakage development and plume migration from the deep formations to the shallow aquifer. Askar et al.[47] addressed these challenges by developing a novel experimental tank setup. First, they showed that the vertical brine leakage under natural settings can be simulated in a horizontal soil tank by using an extremely low concentration of the brine surrogate that can minimize the density-contrast effects on the plume transport. To determine the threshold of the brine surrogate concentration (i.e., NaBr tracer) that can trigger such density effects in the tank, nondimensional density-instability relationships were incorporated with a density-dependent FEFLOW-based model. Results of this analysis showed that using NaBr tracer with a concentration less than 100 ppm nearly eliminated the density effects. Second, the depths of the geological formations in this problem were downscaled to orders of meters to fit the laboratory settings; three distinct zones were included in the soil tank to represent the storage zone (Zone 1), intermediate overlying formations (Zone 2), and the shallow aquifer (Zone 3). These zones were heterogeneously packed using six well-characterized sands.[47] Zones 1 and 3 were packed to represent spatially correlated permeability fields, while Zone 2 was packed as a layered stratified system. Finally, four boundary conditions (BCs) were assigned at both ends of the tank (Fig. 1) to generate multidimensional and interactive flow fields over the three distinct zones of the tank as expected under field conditions. Figure 1 illustrates a schematic of the conceptualized upward brine leakage in the field and the horizontal soil tank used to simulate the vertical brine leakage. Figure 1 also shows the packing configuration, measurement instruments, potential extraction locations, and the BCs used in the experiments.

The soil tank has internal dimensions of 800 cm × 123 cm × 6.5-8.0 cm (length × height × width). The top boundary of Zone 1 was connected to a peristaltic pump (Neuman BC), while both boundaries of Zone 3 were connected to constant head reservoirs (Dirichlet BC). The bottom boundary of Zone 1 was assigned no-flow conditions. By adjusting these BCs, the flow in the tank and across Zone 2 were controlled; the flow in Zone 2 was determined by the overall head difference between Zones 1 and 3. All other sides of the tank were sealed. The front walls of the tank were transparent to facilitate visual tracking the dyed plume and help developing sampling strategies. For more details on the problem conceptualization, experimental design, tank construction, and packing procedures, refer to Askar et al.[47,54]

A total of 695 self-sealing septa ports were installed in one side of the tank for extracting samples to track the plume; out of which, 480 were located at Zone 3 representing the shallow aquifer, while the rest were scattered in Zones 1 and 2. The tank was also instrumented with 30 manometers for hydraulic head measurements; nine of which were in Zone 1 and were designed to be used for both head measurement and fluid extraction. In addition, seventeen extraction wells were placed in Zone 1 so that each of them is located within a different sand type in the random heterogenous packing. This makes the total number of potential extraction wells located at Zone 1 equal to 26 (as shown in the inset part of Figure 1). Fractures were represented in the tank by six 4-cm diameter holes drilled in the acrylic impermeable sheet separating Zones 1 and 2 mimicking the confining caprock. To inject the tracer, six external tubes were placed at the outflow side of the caprock holes (Zone 2). The tracer was prepared using 20 grams of NaBr salt (Mallinckrodt 0535-102.9 NaBr/mol) with 0.03% (by volume) of fluorescence dye (ACROS-Organics 17324-5000) and mixing with ∼171.6 L of tap water. This resulted in a concentration of NaBr tracer around 101 ppm.

Modeling the simulated leakage in the tank

To apply the simulation-based optimization method, a numerical model is needed in conjunction with the GA for performing the forward simulations. The finite element transport code of FEFLOW (V 7.1) was used to develop a 2D flow and transport model to simulate the leakage experiment. The FEFLOW code was validated by Askar et al.[47] for its ability to capture the migration of a NaBr plume under multidimensional complex flow fields in the same tank setup used in this study. The tank domain was discretized in the developed model using 281,591 elements to obtain a high-resolution velocity field in Zone 1 and in the source vicinity for convergence enhancement of the optimization problem. Steady-state injection and transport conditions were assumed in the model for two reasons: (1) minimizing the computational burden of the optimization process; the forward model must be run thousands of times by the GA to find the optimum solution, and (2) capturing the most critical distribution of the plume over Zones 2 and 3, which happens only when the plume occupies the entire area of the tank after reaching steady-state conditions.[47]

Birkholzer et al.,[12] Cihan et al.,[19] and González-Nicolás et al.[20] recommended designing the extraction scheme when more accurate data become available on the deep geological settings and hydrogeological regime. To be consistent with this degree of system characterization, the packing heterogeneity of the sand media in the tank was explicitly represented in the forward model underlaying the GA in this analysis. The initial hydraulic conductivities (*Ks*) of the different sand types were assigned in the model according to the column-scale determined values presented in Askar et al.[47] While the *Ks* of the six caprock fractures were given an initial value of 1.0 m/d in the model. The permeabilities of the potential leakage pathways in an actual GCS site can be estimated using integrated geophysical and geomechanical modeling investigation tools, as discussed later in this section. The sand porosities (ϕ) in the three zones were assigned an average value of 0.4. The longitudinal and transversal dispersion coefficients ($\alpha_L = 0.14$ cm and $\alpha_T = 0.01$ cm for the entire domain) were specified in the model based on the empirical formulas of Neuman.[57] The *K*-field of the model was then calibrated using the preinjection/leakage data of hydraulic heads, inflows, and outflows (i.e., mimicking the collected data from the monitoring system in the field prior to any leakage onset) using the inversion code of PEST.[58,59] The calibrated model exhibited a good fit to the observed heads and flows, prior to injection, with low root mean square errors (RMSE) (i.e., RMSE = 2.87 mm for hydraulic heads and RMSE = 0.02 m^3/d for the tank in- and outflows). It should be noted that the hydraulic and structural properties of Zone 1 and caprock were assumed unknown for a stochastic analysis, presented in section Stochastic Assessment, to validate the use of the proposed design approach under extreme uncertainty in field data.

The latest advances in geophysics have enabled identifying the potential locations of pressure-driven fractures in rock systems and predict their hydraulic properties by integrating seismic data with machine learning and geomechanical models.[60–65] By applying similar techniques in GCS sites, the location of the future damage zones in the caprock can be predicted, and the potential leakage rate via the fractures in these zones can be inferred. Therefore, in this analysis, the potential leakage sources (i.e., the injection ports in the soil tank) were predefined in the forward model as mass influx elements with an assumed injection/leakage rate of 7.9 ml/min and tracer concentration of ∼78 ppm. It should be noted that the used tracer concentration in the experiment was slightly higher than 78 ppm to introduce some uncertainty in the described mass flux in the model as expected under field conditions.

Multiple potential damage zones and leakage sources may be predicted by the integrated geophysical-geomechanical investigation tools discussed above. Due to the high installation cost of deep extraction systems, the optimization algorithm needs to find the best well locations and extraction rates that can control the leakage from any of the identified potential leakage sources. Therefore, in this analysis, three forward models simulating the leakage from various sources were set to run simultaneously under the GA to find the optimum extraction scheme that can control any of these leakage events in the tank. Figure 2(A) presents the three hypothetical leakage scenarios considered in the optimization process. The figure also shows the locations of all potential extraction wells, assigned BCs, and the calibrated *K*-field using the preinjection hydraulic head and flow data.

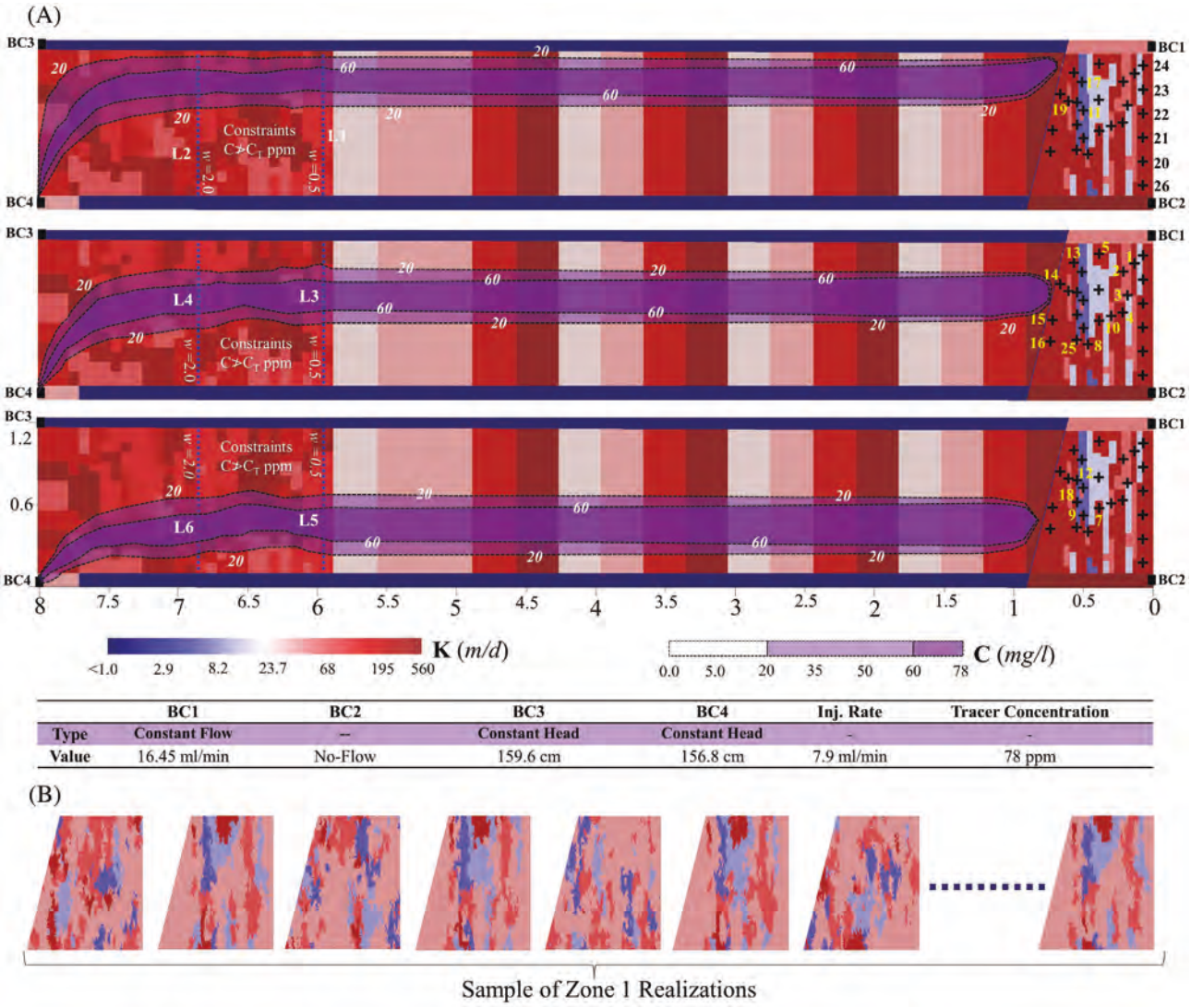

Figure 2. (A) The three forward models, used by the GA in the optimization problem, including the boundary conditions, potential extraction wells, calibrated K-field and the location of the concentration constraining points (Blue dashed lines). The locations of the potential extraction wells in Zone 1 are symbolled by the black crosses. L1-L6 highlights the constraining points at which the concentration profiles of the analysis in section Optimality Check were developed. (B) A sample of the generated realizations of Zone 1 *K*-filed. Note the flow direction is from right to left and (A) and (B) use the same colorscale for the *K* values.

Optimizing the extraction system in the tank

The GA was applied to select the best two extraction wells, out of the 26 potential wells in Zone 1, that can control the leakage that may occur from any of the three potential sources considered in the forward models (i.e., injection ports number 1, 3, or 5). The GA was also allowed to select a single extraction well if such solution results in the lowest required pumping rate to control the leakage plume. A total of 32 constraining points were prescribed in Zone 3 to regularize the objective function by defining the maximum allowed contaminant concentration in the shallow aquifer (e.g., MLCs or NITVs). The constraining points were divided into two 1D vertical arrays located at $X = 5.76$m and $X = 6.83$m (marked by the blue dashed lines in Fig. 2A). These arrays are denoted as "Constraining Group #1 and #2" in Fig. 1 and henceforth. The locations of these constraining groups (CGs) were chosen to represent the deepest and

mid-level strata of the shallow aquifer in the field. Target concentrations (C_T) of zero ppm were assigned to these CGs with different weights (w); $w = 0.5$ was given to the points in the CG #1, while $w = 2.0$ was given to the points in the CG #2. The points in the CG #2 were given a higher weight in the objective function because of their proximity to the shallow aquifer, which makes them more critical to be satisfied by the GA solution. These weights are site-specific variables and other factors in the field (that might be required to be met for regulatory purposes) may determine them. Figure 2(A) shows the identification number of each potential extraction well and the location of the CGs relative to the three leakage sources considered in the forward models.

Under such setup of the optimization problem, the GA selected well #24 to be operated on an extraction rate (Q) of 25.64 ml/min to control the leakage in the tank. Well #24 is located upstream of the fractures close to BC1 at moderately permeable sand type (sand 40/50 see Fig. 2A). This was found to be in a good agreement with the finding of Cihan et al.,[19] that the lowest extraction rates will always occur in a highly permeable zone in the storage formation. The selection of Well #24 by the GA, the closest well to the largest fluid source, can be seen as unsurprising solution. However, it is important to mention that with uncertainty in the deep geological settings and BCs (as can be the case in many GCS sites) of the system, this selection changes drastically (sections Sensitivity Analysis and Stochastic Assessment). Thus, determining the optimum extraction location is not a trivial problem as it depends solely on the flow filed in the storage formation and source vicinity. For the validation of the proposed GA-based approach, it was necessary to compromise on the degree of uncertainty incorporated in this analysis and assume some knowledge about the system, otherwise the validation results cannot be effectively interpreted. For example, if a failure happened in controlling the leakage, we would not be able to distinguish whether this failure happened due to a deficiency in the formulated optimization problem associated with the design approach or a lack in the needed knowledge to reproduce the true flow filed near the source. On other hand, finding the optimum control system is a multiobjective optimization problem (i.e., well locations and pumping rates), which makes it even more complicated to be handled intuitionally.

Experiment procedures

The main motivation of the experimental work of this study was to test the selected GA solution (Well #24 and Q = 25.64 ml/min) under an expected margin of moderate uncertainty in field information and measurements (some data about deep geological settings are available). Therefore, moderate uncertainty conditions were considered in the analysis through using relatively inaccurate model predictions to design the extraction system in the tank. Uncertainties were introduced to the model underlaying the GA process by using: (1) uncalibrated transport parameters, (2) estimated K values based on preinjection hydraulic data only, (3) constant porosities of the different sand types in the same zone, (4) smoothed microheterogeneities in the sand packing, and (5) inaccurate initial tracer concentration at the source, to develop the forward model. Due to the excessive cost and long time needed for setting up, collecting data, and performing the chemical analysis associated with laboratory experiments ($\sim$ 1–2 months for each experiment), a single leakage control experiment was conducted to test the GA results under moderate uncertainty conditions. As a part of the validation analysis, the optimality of the GA results was further evaluated using numerically generated synthetic data (section Optimality Check), where perfect knowledge about the system was implicitly assumed for exploring the impact of minor deviations in the implemented optimal solution on the control-system efficacy.

In the leakage-control experiment, injection port #5 was selected to introduce the tracer as it provides the widest and most rapid migrating leakage plume compared to the other sources, as was found by Askar et al.[47] Such plume characteristics offer critical testing conditions for the leakage control system efficacy, which supports the reliability of the validation analysis. Using a single injection port mimics a scenario where one leakage source was activated by the induced injection pressure in the storage zone. Based on the GA results, the pump connected to well #24 was adjusted to provide an extraction rate of 25.62±0.2 ml·min^{-1} during the experiment. An injection rate of 7.9±0.2 ml·min^{-1} and an inflow rate of 16.4±0.2 ml·min^{-1} to Zone 1 were applied. Three peristaltic pumps (Cole-Parmer Masterflex L/S 7526–60) were used to create such injection and extraction conditions. Two constant head reservoirs were used to impose the specified head BCs shown in Fig. 2(A).

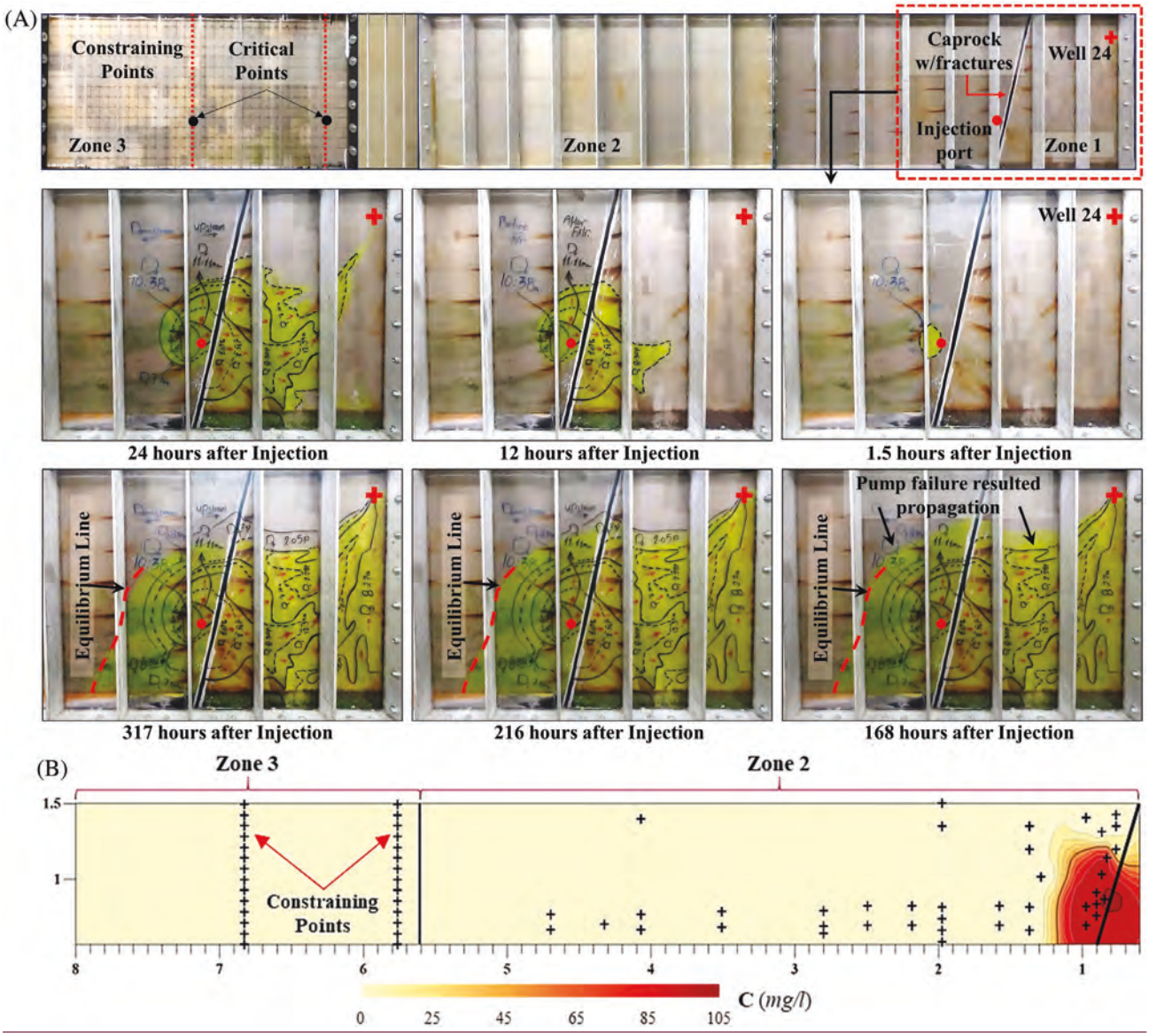

Figure 3. (A) Time-lapse photos of the controlled plume and (B) measured concentrations of the plume at the last day of the experiment.

The injection and extraction processes lasted for 13.2 days of the experiment. In the first 12 days, aqueous samples were collected from the two most critical points in the CGs #1 and #2 (Fig. 3A); these points were identified to be critical based on numerical simulations that revealed their rapid response to the leakage plume generated from port #5. However, on the last day of the experiment (13th day), aqueous samples were collected from all the CGs in Zone 3 besides, 41 ports located at Zone 2 to map the plume extent after control. Collected samples were then analyzed using an ion chromatography system (Dionex Aquion combined with autosampler Dionex As-Dv) following the procedures presented by Askar et al.[47] The hydraulic heads, tank inflow, and outflow were recorded twice a day. A high-resolution camera was used to take time-lapse images of the fluorescein-dyed-tracer every minute to record the plume propagation. The validation analysis was performed by checking whether the prescribed zero concentrations at the CGs in Zone 3 were violated by the controlled leakage.

Experimental validation

The leakage experiment was initiated by injecting the NaBr tracer through port #5 after the background flow in the tank reached a steady state. The extraction phase was not initiated until the leakage plume approached the closest sampling port to the injection point, located 12 cm downstream of the caprock (i.e., the thick-plastic sheet). This scenario mimics a situation of an early leakage detection by deep monitoring sensors that alerted the operators to start the brine extraction system. Although we intended to have a continuous extraction over the entire experimental time, the extraction process was accidentally stopped on the fifth day of the experiment for 3.5 h due to a pump failure. As this is a practical scenario that can occur in the field, the results were used to answer the question: "under unfavorable site conditions of possible failure of the extraction system, can the leakage plume still be controlled and reversed back to the storage formation, if the extraction was reactivated?"

Figure 3(A) shows the development of the plume boundaries with time during the control period of the simulated leakage in the tank (including the pump failure time). The images show that a full control of the plume was achieved by restarting the control system after pump failure: most of the leakage flow was reversed to Zone 1, while only a small portion of the plume propagated in Zone 2 by dispersion. The plume then reached equilibrium after ∼6 days at ∼35 cm from the caprock (red dashed line in Fig. 3A). Collected data over the entire ∼13.2 days of the experiment showed undetectable levels of Br concentrations with the IC (<0.1 ppm) at the two most critical constraining points in the shallow aquifer. Figure 3(B) shows an interpolated concentration map of the leakage plume based on the 13th-day data collected from the 41 ports in Zone 2 and the CGs in Zone 3. As shown in that figure, the plume was controlled and maintained in the vicinity of the source for the entire time of the experiment. These results validate the applicability of using the GA to find the optimum locations and pumping rates of the extraction wells used to control the potential brine leakage from the CO_2 storage formations.

Optimality check

To test the degree of optimality of the GA results, the best extraction scheme (i.e., well #24, $Q =$ 25.64 ml/min) was slightly altered into eight forward simulations to quantify the corresponding impact on the plume concentrations at the CGs in Zone 3. In the first four simulations, the optimum extraction rate ($Q = 25.64$ ml/min) was prescribed to other wells than the selected one by the GA (i.e., wells number 13, 14, 15, and 16). These wells were chosen for this analysis because of their locations at high permeable sand close to the caprock fractures, which can be seen as a promising extraction site to control the leakage plume based on the findings of Cihan et al.[19] In the rest of the simulations, the optimum extraction rate of well #24 was sequentially reduced by 0.1, 5, 10, and 15% in the model. The results of the eight simulations were compared to the optimum solution results under each leakage scenario (i.e., Injection ports number 1, 3, and 5); the plume concentration profiles along the CGs in Zone 3 were compared to the zero-concentration profile obtained by applying the optimal solution (blue solid line), as shown in Fig. 4.

Figure 4 shows that altering the extraction well location (all black lines) significantly affected the control efficacy in the leakage scenario #1 compared to the other two scenarios. This is because the chosen port to introduce the tracer in that scenario was the closest port to the upstream BC in Zone 1 (i.e., BC1). The fluid flux introduced via BC1 together with the injected tracer flow generated a considerably high leakage rate through the upper fractures in the caprock (i.e., openings #1 and #2, see Fig. 1). Hence, the GA selected the closest well to BC1 (well #24) as an optimal solution so that both the flows from Zone 1 to these fractures are hydraulically intercepted (by the imposed negative-pressure during extraction) and the leakage-plume migration is reversed to Zone 1. Under such conditions, the leakage control in scenario #1 became particularly sensitive to the distance between the extraction well and BC1; the further the extraction well is located from BC1, the higher the concentrations of the leakage plume in the shallow aquifer (scenario well 13-Opt.Q versus scenario well 16-Opt.Q). It is important to note that the above interpretation is based on the simulated flow field by the inaccurate forward models used in this analysis (as discussed in section Experiment Procedures), which may not be valid for the actual test system. On a different note, the skewness and variable ultimate values of the concentration profiles in scenario 1 (Fig. 4) indicate a high sensitivity of the controlled plume distribution to the position of the extraction well relative to the storage zone heterogeneity and fracture locations. In addition, the

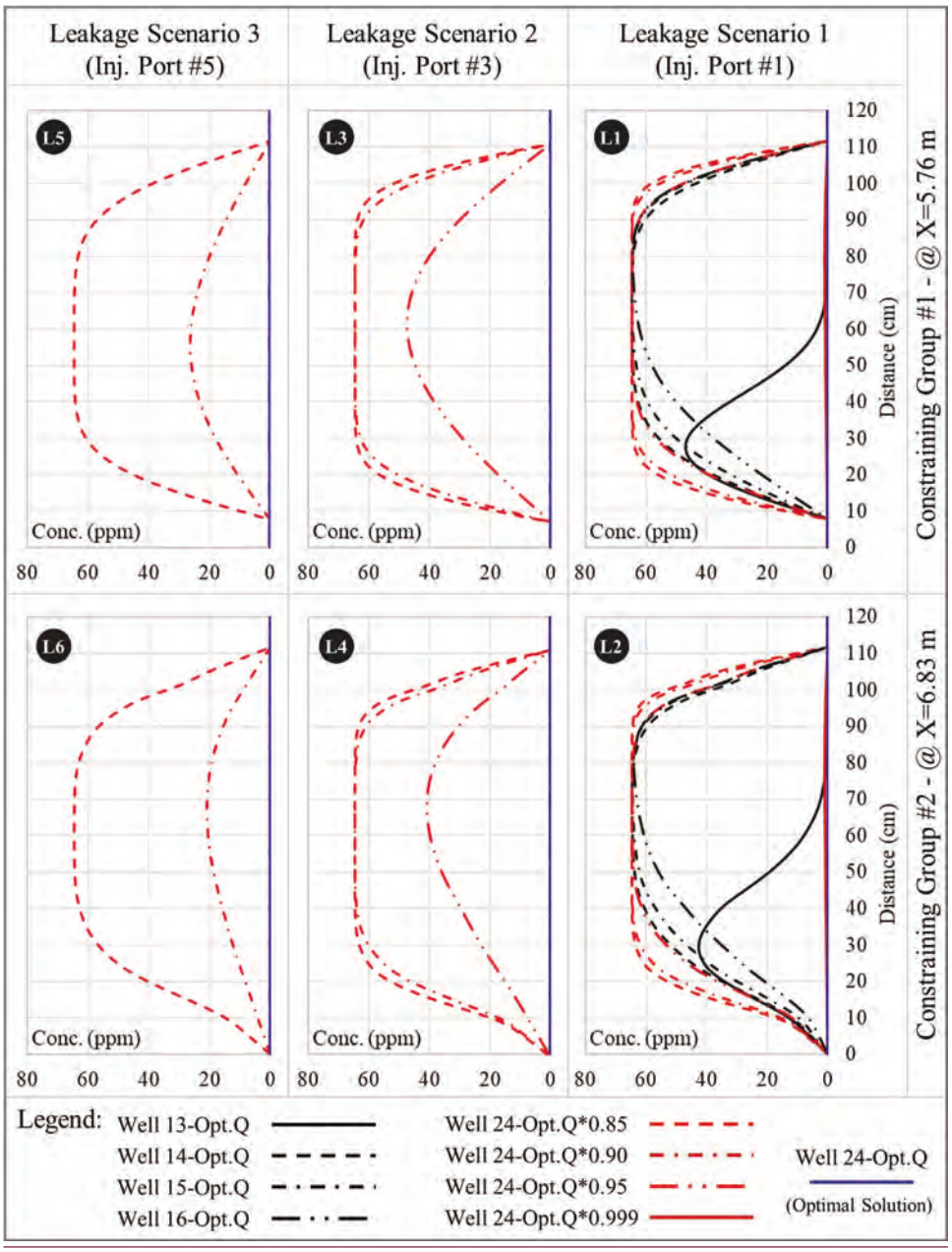

Figure 4. The concentration profiles of the plume at the two sets of the constraining points located at $X = 5.76$ m and $X = 6.83$ m under the considered eight optimality testing scenarios. L1-L6 indicates the locations of these concentration profiles in the model domain presented in Fig. 2(A).

analysis showed that applying lower extraction rates (all red lines) than of those suggested by the GA by less than or equal to 10% can drastically impact the leakage control efficacy under all leakage scenarios, even if the best extraction location was used.

In summary, the results revealed that using any well other than the selected one by the GA (well #24) or reducing the optimal extraction rate (25.64 ml/min), by only 0.1%, can produce a leakage plume that violates the assigned concentration constraints (i.e., $C_T \not> 0.0$ ppm) in the shallow aquifer. This suggests a high degree of optimality of the selected extraction scheme by the GA. The observed sensitivity of the plume concentrations in the shallow aquifer to well location

Table 1. Studied uncertainty scenarios and optimization results.

Categories ($C_T \not> 0.0$ ppm)	Number of scenarios	First Well# (Freq %)	Second Well# (Freq %)	$\mu \cdot Q_1$* (SD) (ml/min)	$\mu \cdot Q_2$* (SD) (ml/min)	$\mu \cdot Q_T$** (SD) (ml/min)
1. Six *K*-Frac. = 1 m/d	1	24 (–)	–	25.47 (–)	–	25.47 (–)
2. Six *K*-Frac. = 500 m/d	1	1 (–)	24 (–)	9.95 (–)	16.69 (–)	25.64 (–)
3. Random *K*-Fractures (1–500 m/d)	12	24 (75%) 13 (17%) 1 (8%)	24 (42%) 1 (33%) 13 (17%) 26 (8%)	13.16 (7.16)	12.43 (7.3)	25.59 (0.58)
4. Conditioned Realizations for Zone 1	10	24 (60%) 1 (30%) 26 (10%)	24 (50%) 1 (20%) 5 (10%) 19 (10%) 23(10%)	15.44 (7.79)	10.38 (7.86)	25.87 (0.12)
5. Unconditioned Realizations for Zone 1	10	24 (80%) 1 (10%) 25 (10%)	24 (60%) 1 (10%) 2 (10%) 3 (10%) 21 (10%)	15.37 (7.44)	10.07 (7.42)	25.79 (0.07)

*μ.Q1 and μ.Q2 refer to the mean extraction rate of the first and second selected wells by the GA.
**The total extraction (Q_T) was always higher than the sum of the tank inflow and tracer injection (24.35 ml/min).

and extraction rate highlights the fact that finding the optimal leakage-control scheme is not a "commonsense" problem due to the nonconvexity and high dimensionality of its solution space.

Sensitivity analysis

Owing to the typical lack of accurate information about the caprock fracture permeabilities and storage zone heterogeneity under field conditions,[66] particularly for sites that have not been explored for oil production, multiple uncertainty testing scenarios, divided into five categories, were performed to examine the sensitivity of the optimization results to these parameters. As shown in Table 1, under categories number 1, 2 and 3 the case of using inaccurate *K*-fractures to develop the forward model underlining the GA was addressed. In the scenarios composing the first two categories, identical *K*s of 1 and 500 m/d were assumed for the six fractures in the model. While under category #3, the scenarios included random *K*-fractures that were sampled from a uniform distribution spanning the values between 1 and 500 m/d. In addition, 20 scenarios were developed under categories #4 and #5 to address the effect of uncertainty in our knowledge about storage zone heterogeneity on well selection and extraction rates. To develop these scenarios, conditional and unconditional geostatistical simulations were performed for Zone 1 ln*K* using the algorithm of sequential indicator simulator in SGeMS.[67,68] Notably, all tested scenarios in this analysis contained a constraint of $C_T \not> 0.0$ ppm in the shallow aquifer (Zone 3).

Table 1 presents the optimization results of all tested scenarios including the frequency of well selection (Freq) as well as the mean (μ) and standard deviation (SD) of the chosen extraction rates. In this analysis, well #1, located 12 cm downstream well #24, was the second most selected candidate under all tested scenarios after well #24. The reciprocal selection between these two wells as optimum solutions, despite their proximity, highlights the key role of storage zone heterogeneity and fracture *K*s in altering the local flow field at the source vicinity, which affects the best extraction location and rate to control the leakage. Moreover, Cihan et al.[19] emphasized that the consistency in well selection (i.e., well #1 and #24) under different problem settings can be a truthfulness indicator of the optimization results.

Well selection was found to be more sensitive to the changes in Zone 1 heterogeneity than fracture *K*s. Minor differences were noticed in the GA results when conditioned and unconditioned realizations were used to define the random field of the storage zone heterogeneity (i.e., categories #5 and #6). This can be attributed to the limited space of Zone 1 that did not allow for generating largely varied heterogeneity architectures in the developed conditional and unconditional realizations. However, a major difference in well selection was noticed when the optimization results of these scenarios (i.e., categories #5 and #6) were compared to the optimal solution (well #24, $Q =$ 25.64 ml/min). This indicates the importance of mapping the permeability field of the storage formation accurately for obtaining an optimum well selection.

Varying the fracture *K*s affected the values of the optimal pumping rates more than well selection (categories from #1 to #2). This is because the fracture *K*s control the leakage flow rate that in turn must be minimized, through brine extraction, to manage the leakage. The effect of fracture *K*s on the optimum extraction rate was much pronounced in category #1, where the reduction in the fracture *K*s decreased the required extraction rate, but did not affect well selection (i.e., well #24). Askar et al.[47] highlighted the role of storage zone heterogeneity and fracture *K*s in determining the leakage pathways, which supports the above findings. The results show an overall high sensitivity of the optimal solution to the changes in storage zone heterogeneity and fracture *K*s because both parameters control the local flow field at the vicinity of the source.

Stochastic assessment

The above sensitivity analysis highlighted the importance of running the optimization algorithm several times under different realizations of the system properties, especially the caprock and storage zone settings, to find the optimal control system under uncertainty conditions. Therefore, in this analysis, the GA was applied in a stochastic framework and tested under the assumption that the hydraulic and structural settings of Zone 1 and caprock fractures are unknown. For this analysis, 166 steady-state forward models were developed to include different realizations of the ln*K* filed of Zone 1 (Fig. 2B). In these models, the *K* values of the six caprock fractures/openings were randomly sampled from a uniform distribution spanning the values between 1 and 500 m/d. Although, there can be a margin of uncertainty in the predicted fracture locations, varying the *K*-fractures was considered enough to proxy this type of uncertainty, as both parameters control the local head and flow distributions at the source vicinity that govern the plume downstream migration.[47] Moreover, uncertainties in the system BCs were also considered in this analysis through altering the assigned Neumann and Dirichlet BCs in the models by ±4%. It should be noted that ±4% was the maximum margin of variation that can be considered so that the flow direction in the tank is not reversed from Zone 3 to Zone 1.

The sand heterogeneities in Zones 2 and 3 were assumed known and were explicitly represented in the models according to the packing configuration in the tank. The notion of this assumption is centered around our ability to map the interfaces between the overlying formations and the heterogeneity of the shallow aquifer in the field using geophysical techniques with sufficient accuracy.[69–71] The 166 forward models were not calibrated on any preinjection data. Hence, the column-scale determined *K*s of the different sands and presented in Askar et al.[47] were used to define the *K*-filed of Zones 2 and 3 as well as developing the realizations of Zone 1. The three potential leakage plumes were simultaneously simulated under each model, as discussed in section Optimizing the Extraction System in the Tank. The GA was then applied to successively solve for the best two extraction wells that provide the lowest pumping rates to control the three leakage plumes under each model.

Figure 5 presents the GA stochastic results for the developed model/parameter ensemble. Figure 5(A) shows the selected well combinations by the GA across the 166 models; points are color-coded based on the selection frequency (light gray and dark red indicate low and high selection frequency, respectively). Figures 5(B) and (C) demonstrate the histograms of the optimum pumping rates of each selected well. While Figure 5(D) shows the cumulative probability density function (CDF) of the total extraction rate needed to control the leakage plumes.

In general, the results confirm the sensitivity analysis findings by exhibiting a wide range of optimum solutions in terms of extraction well locations (Fig. 5A) and pumping rates (Figs 5B and C). It should be noted that all extremely low extraction rates presented in Fig. 5(B) for the first selected well (< 1.0 ml/min) are associated with high extraction rates from the second selected well (Fig. 5C) and vice versa. This can also be interpreted from the CDF plot in Fig. 5(D), which shows that the lowest total extraction rate resulted from the 166 GA runs is 16.85 ml/min. Figure 5(A) suggests that Well #24 was the most frequently selected single-well by the GA to control the three leakage plumes (selected 34 times), which is in a perfect agreement with the GA deterministic results (section Optimizing the Extraction System in the Tank). While Figure 5(C) reveals 75% confidence that the *Q*-range of 24.2–28.8 ml/min will include 80% of the optimum extraction rates. This range and even smaller (the range associated with the 50% confidence interval) are both bracketing the experimentally validated extraction rate of 25.64 ml/min. These results indicate a successful implementation of the proposed design approach

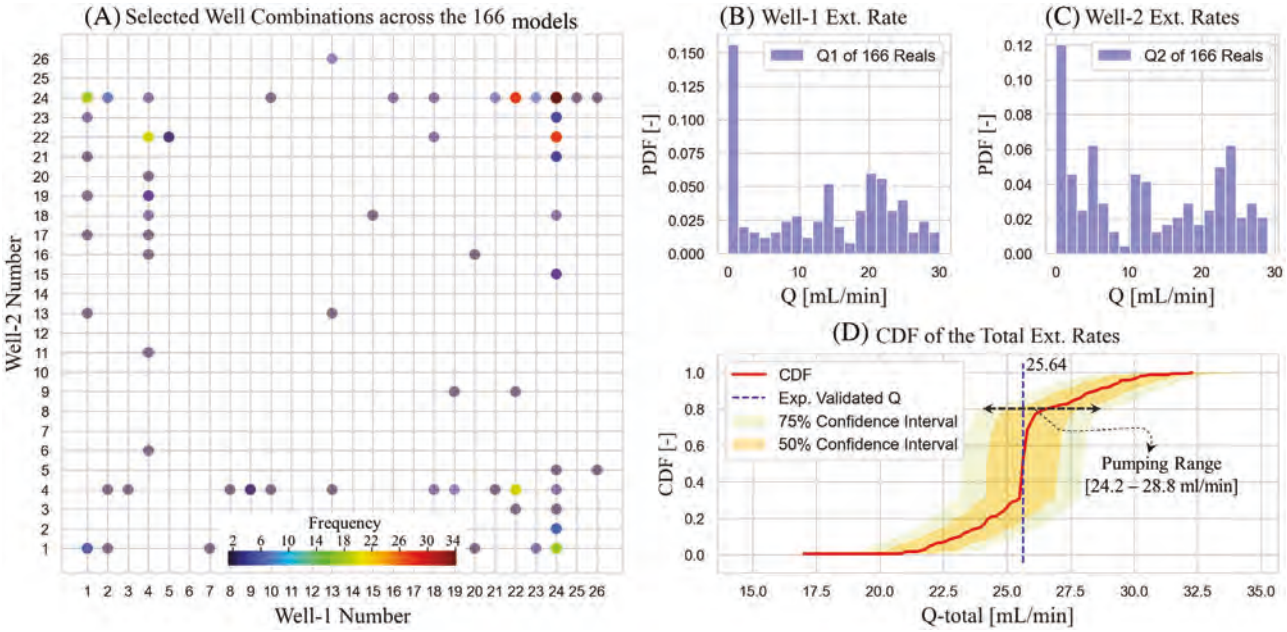

Figure 5. GA stochastic results including (A) the selected well combinations, (B, C) histograms of the optimum extraction rates from each selected well, and (d) CDF of the needed total extraction rates from the system. Reals stands for realizations.

under extreme uncertainty conditions, as we were able to determine the correct optimum extraction location and a plausible range of extraction rates to be used.

Birkholzer et al.,[12] Cihan et al.,[19] and González-Nicolás et al.[20] suggested a metric referred to as the brine extraction ratio to assess the practicality of the extraction system for field implementation. This ratio describes the volume of native brine needs to be extracted relative to the volume of CO_2 planned to be injected. This ratio should be less than unity for the extraction technique to be practical. Despite the ability of controlling the experimental conditions in the intermediate-scale system to mimic the physical processes in the field, there were limitations to assess such practicality using the laboratory experiment only. This is because the leakage flow through the constantly opened six fractures in the tank is controlled by the head gradient between Zones 1 and 3. Thus, to control the leakage and contain the plume in Zone 1, this hydraulic gradient should be reversed towards Zone 1. Since this condition cannot be accomplished except when the extraction rate from Zone 1 exceeds the sum of tank inflow (through BC1) and tracer injection, the extraction ratio will always be greater than one. Therefore, it was essential to evaluate the practicality of the extraction technique under field-like conditions, where only a portion of the lateral flow in the storage zone (i.e., native brine) is expected to leak from activated caprock discontinuities. This evaluation was performed using numerical modeling as discussed in the next section.

Numerical testing

As the experimental validation was limited to a system downscaled from field setting, additional analyses were conducted using numerical modeling at a realistic scale of GCS application. For this hypothetical analysis, the potential CO_2 storage site at the Vedder formation in San Joaquin Basin, California was selected. Extensive information on the hydraulic properties and geologic settings of the San Joaquin Basin and Vedder formation are available from past studies associated with oil and gas exploration[72] and GCS assessment.[49,50,73,74] The Vedder formation consists of permeable sandstone layers that dip upward towards the Sierra Nevada mountain-range located near to the eastern boundary of the San Joaquin Basin. The Vedder formation is overlaid by double caprock shale layers (i.e., Freeman Shale and Fruitvale Shale) with an average thickness of about 300 m for each. Figure 6(A) shows a simplified cross-section of the San Joaquin Basin that was originally developed by Oldenburg et al.[75] based on the data provided by Downey and Clinkenbeard.[76] The

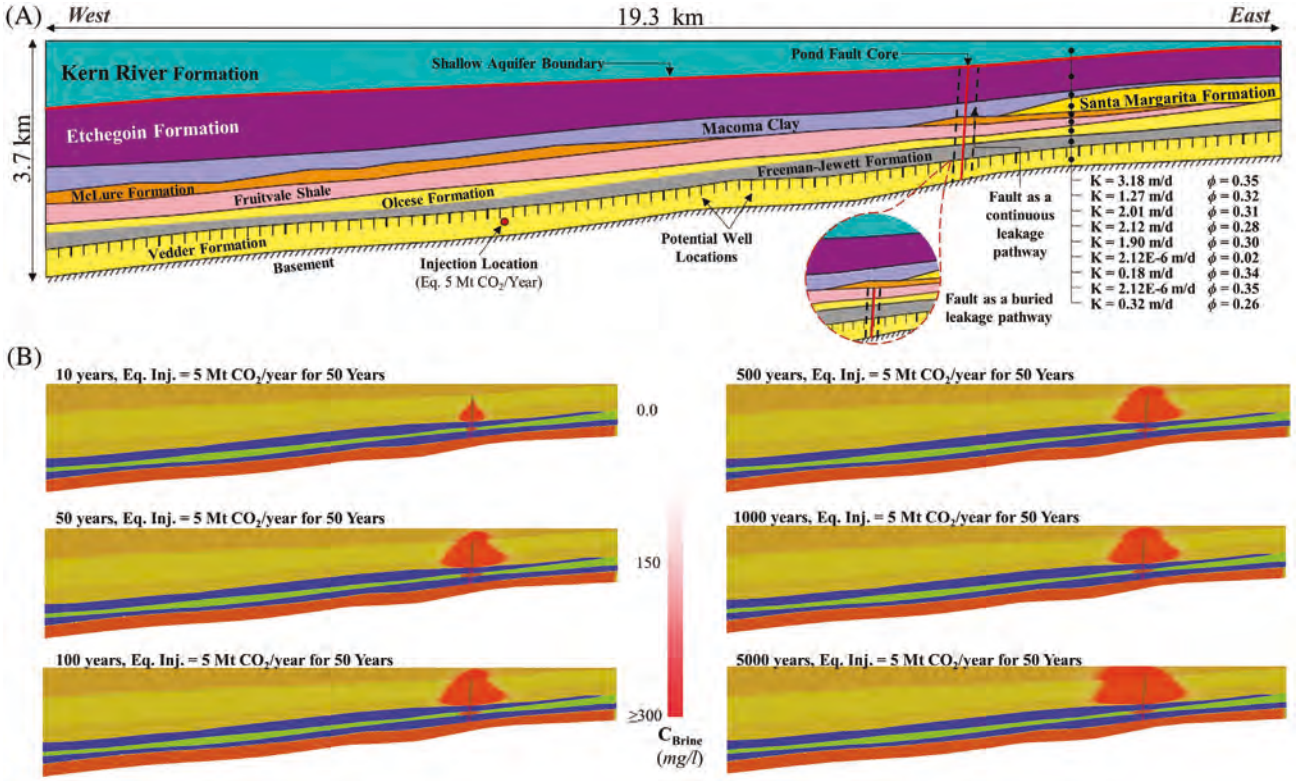

Figure 6. (A) simplified cross-section of San Joaquin Basin stratigraphy and (B) transient simulation of the leakage plume propagation after fault activation by the equivalent injection of 5 Mt CO_2/year for 50 years.

most reported injection site in the literature is located ~7.2 km west of the Pond fault in the Vedder formation.

The Vedder formation storage capacity for a CO_2 injection scenario with a rate of 5 Mt CO_2/year for a period of 50 years was tested numerically by several researchers.[49,73,77] Most of these studies emphasized that the existing faults within the project area of review (refer to Ref. [78]) can be subject to a significant pressure increase, which may cause fault activation, induced seismicity, and thus brine/CO_2 leakage. Therefore, Cihan et al.[19] and González-Nicolás et al.[20] studied the possibility of implementing a brine extraction system to manage the build-up pressure in the Vedder formation. On the other hand, Jeanne et al.[74,79]) focused on assessing the stability of the Pond fault and overlaying formations under such an injection scenario. They found that the occurrence of a large earthquake because of this injection scenario is unlikely, but low-magnitude frequent seismic events can be expected to happen. Microseismic events may not represent a significant geomechanical risk on the overburden formations, but during such events, the Pond fault permeability can increase and act as a hydraulic pathway.[21,22,80,81] In contrast, Jeanne et al.[82] showed that a succession of fault-slip events due to a series of microseismic activities will not always generate a fully activated conductive pathway. They also found that during a fault activation, the permeability behind the rupture propagation is higher than its front, which can result in a pathway that include a more conductive interval close to the pressure source (i.e., storage formation).

In the same context, the numerical studies of Guglielmi et al.,[83] Cappa et al.,[84] Rutqvist et al.[85] and Park et al.[86] demonstrated a reasonable occurrence probability of deep fault opening, close to the storage formation (i.e., highest pressure Zone), due to the reduction in the effective normal stresses in the caprock after CO_2 injection. Such opening can impose a considerable variation in the permeability of the deep and shallow parts of the activated fault. Moreover, immediately after activation, the migrating high-velocity fluids through the fault can fluidize the sandy internal surfaces of its segments located in the overlying sandstone formations of the San Joaquin

Basin.[87] This process can significantly reduce the permeability of the fault upper segments, which will limit the conductive part of the fault to the length between the Vedder formation and the top boundary of the caprock (i.e., Fruitvale Shale). A comprehensive review on fault activation and hydraulic pathway creation associated with GCS operations can be found in Guglielmi et al.[88]

Based on above, the Pond fault may act as a continuous leakage pathway extending from the storage formation to the shallow aquifer,[89] or as a buried pathway (e.g., deep thrust faults in Boston et al.[90] overburdened by the sandstone layers (i.e., Etchegoin and McLure formations). In other words, the Pond fault can transfer the Vedder formation brine right above the caprock units (i.e., functions as short conduit or buried leakage pathway) or directly convey the brine mass the whole way up to the shallow aquifer (i.e., functions as deep conduit or continuous leakage pathway). Leakage through a continuous pathway is expected to be advection dominated with minimal lateral dispersion in the system. While the propagation of a leakage plume from a buried pathway will be governed by both advection and dispersion due to its interaction with overlying groundwater regimes and surrounding units. Advection-dominated transport can be controlled by reversing the upward leakage flow through the created pathway without relying on the dilution capacity of the overlying formations. However, to examine the benefit of this dilution capacity, both potential settings of the Pond fault after activation (i.e., continuous or buried pathways) were considered. The GA was used to find the optimum location and pumping rate of an extraction well that can control the hypothetical brine leakage event from the Vedder formation so that the plume concentrations in the shallow aquifer do not exceed a specified limit.

Modelling simplifications and assumptions

Large-scale 3D multiphase models are computationally intensive and can present a significant obstacle to be used as forward models in optimization problems.[91] The question here "Do we need such degree of model complexity to simulate a far-field brine leakage from a CO_2 storage zone?" Generally, researchers apply different types of simplifications to reduce the computational burden of the models without significantly affecting the prediction accuracy. For example, in the context of deep leakage problems, Gassiat et al.,[80] Jeanne et al.,[92] Huang et al.,[93] and Vialle et al.[66] used 2D vertical cross-sectional models to study CO_2 and brine leakage problems. This is because the large variability in the geological settings along the vertical direction is central to the upward plume migration compared to variations in the lateral direction. Since this study focuses also on the vertical migration of far-field brine leakage, we used a 2D vertical cross-sectional model to simulate the hypothetical leakage problem in San Joaquin Basin.

Regarding the distinct phases of flow that need to be considered for modeling brine leakage, Cihan et al.[94] showed the suitability of using a single-phase flow model to simulate far-field flow and brine leakage. In addition, a review article by Bandilla et al.[95] reported the validity of using a single-phase model to simulate the pressure response and flow dynamics at distant areas from the supercritical CO_2 plume. Examples of single-phase models used in exploring GCS-related problems include Nicot[96] and Zhou et al.[97] It is worth mentioning that Cihan et al.[19] simulated the pressure build-up at the Vedder formation through applying the multiphase flow equations within a square of 15×15 km^2 only from the model grid, which was much smaller than the full domain size of 84×112 km^2. This is because the CO_2 plume migration distance in the Vedder formation was found smaller than this square size as reported by Cihan et al.[19] Therefore, single-phase flow conditions were assumed in our model to simulate the Vedder formation pressure build-up and the upward brine leakage that follows through the Pond fault.

To enable the single-phase flow assumption, a brine injection equivalent to the actual CO_2 injection needs to be considered. Cihan et al.[94] found that the corresponding changes in the volumetric CO_2 injection rate due to pressure-driven variations in the fluid properties (CO_2 density) are minor. Therefore, they applied a constant-rate equivalent fluid/brine injection to represent the CO_2 injection in a single-phase model. Their single-phase model resulted in sufficiently accurate pressure build-up in the storage formation and brine leakage rate compared to the sophisticated multiphase flow model. Thus, an equivalent constant-rate brine injection was used in our model to represent the actual CO_2 injection in the field. To ensure reproducing a comparable pressure field to the 3D model of Cihan et al.,[19] the prescribed equivalent injection rate in our model was adjusted

until a similar pressure build-up to Cihan's model was obtained under the Pond fault. By that, a reasonable simulation of the pressure-driven brine leakage at the vicinity of the Pond fault due to the injection scenario of 5 Mt CO_2/year was guaranteed.

The Vedder formation has salinity levels that range between 100 to 29,000 ppm, with an average brine density around 989 Kg/m^3.[19,50] Due to the minimal difference between the densities of the formation brine and overlying groundwater (i.e., 998 Kg/m^3), density-independent flow conditions were assumed in the 2D model. All above model simplifications were necessary to reduce the computational burden of the forward simulations need to be executed during the optimization process.

San Joaquin basin model setup

The simulation code FEFLOW was used to develop the 2D flow and transport model of San Joaquin Basin with the domain dimensions presented in Fig. 6(A). A total of 675,025 mesh elements with an average size of ∼77 m^2 were used to spatially discretize the problem domain. A mesh refinement was applied at the fault vicinity to improve model convergence; the smallest mesh size in this zone was around 0.001 m^2. The basin stratigraphy shown in Fig. 6(A) was explicitly represented in the model. The values of the formation specific storages, *K*s, and porosities (Fig. 6a) were retrieved from Cihan et al.[19] and Jeanne et al.[74] Following Jeanne et al.,[74] constant hydraulic heads were prescribed at the model boundaries while assuming initial hydrostatic pore pressure in the flow model. An overpressure of ∼96 kPa was imposed in the Vedder formation through the assigned BCs to mimic the typical confinement conditions of storage formations in the field.[98,99] Adverse lateral hydraulic gradients, with the same value of 25×10^{-7}, were assigned to the overlying formations and storage zone in the model. Given the opposing effects of temperature and pressure on the brine density with depth, isothermal conditions were assumed in the model similar to Birkholzer et al.[73] The longitudinal and transversal dispersion coefficients were prescribed as 246 and 24.6 m, respectively, based on the formulas suggested by Neuman[57] and Gelhar et al.[100]

Widths of 1.0 m and 100 m were used to describe the fault core and its surrounding damage zone, respectively. Notably, the geomechanical deformations in high-porosity sandstone result in a permeable fault core, acting as a flow conduit, and a less permeable surrounding damage zone.[101–103] Since most of the geological formations of the San Joaquin Basin are composed of grained sandstone,[104] the *K* of the Pond fault core after activation was assumed two orders of magnitude higher than the average of the *K*s in the system. While the *K* of the damage zone was assumed lower than its adjacent formations' *K*s by two orders of magnitudes, following Gassiat et al.[80] This configuration of the *K* values in the model was applied to represent the Pond fault as a continuous leakage pathway (i.e., the first setting) (Fig. 6A). However, to represent the Pond fault as a buried leakage pathway (i.e., the second setting), the formations overlaying the Fruitvale Shale caprock were connected across the fault zone as shown in the inset part of Fig. 6(A). Reservoir salinity was prescribed in the model by interpolating the TDS concentrations between the eastern and western sides of the study area over the model nodes (i.e., 100 and 29,000 ppm, respectively).

Optimization problem description

Brine leakage through a continuous pathway (e.g., a leaky fault or well connecting the shallow aquifer with the storage formation) can be faster and riskier than that from a buried pathway (e.g., a thrust fault or a damage zone in the caprock). This is because the plume from the latter will encounter multiple overlying formations before reaching the shallow aquifer which will disperse and dilute the plume concentrations. Therefore, to explore the extent of the potential areas to be impacted by brine leakage in the shallow zone of San Joaquin Basin (i.e., Kern River formation), a 2D model representing the fault as a continuous leakage pathway was initially run under transient flow and transport conditions for 5,000 years. Figure 6(B) illustrates that the brine leakage can reach the shallow aquifer with a concentration higher than 300 ppm in less than 50 years (before the end of the injection phase). Therefore, implementing a leakage control system that uses brine extraction wells can be a feasible solution to maintain a continuous injection process and protect the shallow aquifer from a contamination risk.

For optimizing the locations and extraction rates of these control wells for both potential leakage mechanisms in the system (i.e., through a continuous or buried leakage pathway), a steady-state flow and transport model was used under the GA to avoid the computational capacity required for running the

Table 2. San Joaquin basin optimization result.

	Continuous pathway		Buried pathway	
Target concentration at shallow aquifer (C_T)	Selected well number	Extraction ratio × 100 (%)	Selected well number	Extraction ratio × 100 (%)
$C_T \not> 0.1$ ppm	73	47.31	73	47.19
$C_T \not> 0.5$ ppm		47.26		46.94
$C_T \not> 1.0$ ppm		47.22		46.78
$C_T \not> 5.0$ ppm		47.02		46.12
$C_T \not> 10$ ppm		46.85		45.51
$C_T \not> 20$ ppm		46.61		43.62

transient model numerous times (in some cases more than 1000). Under steady-state conditions, the reduction in plume concentrations caused by the infinite dispersion and diffusion process of the plume, is opposed by the enhanced advective transport of the leakage due to the applied continuous injection in this model. This results in a more distributed leakage plume across the overlaying formations, but with slightly lower maximum concentration compared to the transient model results (i.e., 20% lower). Even though this model can be seen as unrealistic, it was considered satisfactory for the purpose of the current analysis conducted to explore both the practicality of the leakage control method (i.e., the extraction ratio) and the sensitivity of the extraction rates to the target concentrations in the shallow aquifer.

A total of 97 potential well locations were predefined along the stretch of the Vedder formation for the GA selection, labeled from 1 to 97 starting from the western side (Fig. 6A). The potential well locations were separated by 200 m. The optimization problem was constrained by a set of target concentrations (C_T from 0.1 to 20 ppm) of the leakage at the interface between the shallow aquifer and its underling formation (marked by a thick red line in Fig. 6A). Different C_Ts were evaluated to explore the impact of regulators' choice regarding the contaminant maximum concentration in the shallow aquifer (e.g., MCLs or NITVs) on the optimization results. The NITVs can be higher than the MCLs of EPA in some cases;[62] for example, when the shallow aquifer contains brackish water (e.g., costal aquifers) or is already impacted by another contamination source, which gives the regulators a chance to increase the C_T. The chosen maximum allowed concentration of the leakage in the shallow aquifer should also be tied to the quality of brine in the storage formation and the expected geochemical reactions along its travel distance to the shallow aquifer. For example, if native brine contains or is expected to dissolve significant amounts of hazardous trace metals (e.g., As, Pb, Cd, etc.),[31,105,106] reasonably low C_T is expected to be chosen for the shallow aquifer.

Optimal extraction system for the Vedder storage

Table 2 presents the selected extraction wells by the GA with their corresponding extraction ratios to control the leakage under both potential leakage mechanisms in the system (i.e., through a continuous or buried leakage pathway). Recall that the extraction ratio describes the required extraction rate to control the leakage relative to the equivalent injection rate of CO_2. Note that since a steady-state model was used in this analysis, the extraction and injection rates are directly related to the extracted and injected volumes of brine and CO_2, respectively. Following Birkholzer et al.,[12] Cihan et al.,[19] and González-Nicolás et al.,[20] such extraction ratio was used as a metric to evaluate the practicality of the extraction technique to control a brine leakage event. As shown in Table 2, the GA selected well #73 for all tested scenarios of plume target concentrations under both potential leakage mechanisms in the system. Such replicated selection of the same extraction well suggests that with a single pathway in the caprock and a homogeneous permeability field of the storage zone, the closest well to the leakage pathway becomes the optimal solution. This confirms the importance of accurately

representing the storage zone heterogeneity in the forward model underlying the optimization problem to find the best extraction location.

The results presented in Table 2 reflect below-unity values of the extraction ratios (i.e., less than 50%) that indicate the practicality of the extraction technique to be implemented in the field. Moreover, the extraction ratios were found decreasing with higher target concentrations (C_T) at the shallow aquifer. Such decrease was much pronounced under the buried leakage pathway scenario compared to the continuous leakage pathway, where increasing the C_T from 0.1 to 20 ppm reduced the required extraction rate by ∼1.5% under the later scenario versus ∼8% under the former one. This difference can be attributed to the fact that the leakage transport through a continuous pathway is advection dominated. While the propagation of a leaking brine from a buried pathway is governed by both advection and dispersion, which allows for the utilization of the dilution capacity of the overlaying formations. It should be noted the results of the extraction ratio and well location are expected to change with different definitions of the system hydraulic and structural properties, as discussed in section Experimental Analysis. However, in this analysis, the authors applied the most frequently used parameters to define the San Joaquin basin so that the applicability of implementing the extraction technique in the field is tested under one of the common realizations of the system in literature.

For extending this analysis, the extraction ratio results were fitted to a first-order polynomial with R^2 greater than 0.95 (Fig. 7A). This regression analysis showed that with increasing the C_T to 50 ppm only, the extraction ratio can be reduced in the buried pathway scenario five times more than it is in the continuous pathway scenario. Since the extraction ratio can be directly translated to the pumping rate required to control the leakage, the results indicate that managing a leakage from a buried pathway can be less expensive than a leakage from a continuous pathway. However, when the required C_T at the shallow aquifer is extremely low (0.1 ppm), the extraction ratios under both leakage mechanisms become similar (Fig. 7A and Table 2). This is because in the case of low C_T, the leakage flow from the source should be totally eliminated, which can be only accomplished by reversing the entire leakage flow to the storage zone, regardless the pathway setting.

Figures 7(B–E) illustrate the plume concentration profiles under both potential leakage mechanisms at the bottom boundary of the shallow aquifer (marked by a red line in Fig. 6A) when the extraction well #73 was operated on the optimum extraction rates. As shown, the GA suggested optimum extraction rates that maintain the plume concentrations in the shallow aquifer lower than the predefined target values in all tested scenarios. By comparing the concentration profiles in Figs 7(B) and 8(C) with Figs 7(D) and (E), a more dispersed plume by the lateral flow of the overlying formations can be noticed in the scenario of a buried leakage pathway. This confirms the efficient utilization of the dilution capacity of the encountered overlaying formations by the plume under this scenario. However, the sharp concentration spikes observed in the plume profiles under the continuous leakage pathway scenario indicate a minimal dispersion effect on the controlled plume (Figs 7B and C). It is worth mentioning that the dilution capacity of the overlying formations is expected to change with time, formation depths and soil type. Moreover, the findings related to the continuous and buried leakage pathway mechanisms can be extended to leaky well and fracture leakage cases, respectively, as these mechanisms generate leakage plumes that will experience similar transport conditions. Since number of researchers represented the leaky wells as highly permeable porous media in their numerical models,[107–113] the approach presented herein can be adopted to control the leakage through abandoned wells existing in the areas of review of GCS operations.

The primary goal of this analysis was to evaluate the applicability of using the extraction control system under a realistic scale of the leakage problem, which was not available to be addressed using the experimental setup. Therefore, the authors did not consider any heterogeneity in the Vedder formation or the potential of having multiple leakage pathways in the system, as the impacts of these factors on the GA results were already explored in Section 3.

Many important questions may arise regarding the management of actual near-field brine leakage problems that will need future work, beyond the scope of this applicability testing analysis, to be answered. For example, a multiphase modeling effort is required to evaluate what will happen to the CO_2 entrapment in the storage formation when the extraction well is under operation, how much CO_2 will be produced by the extraction wells, and what are the impacts on the GA

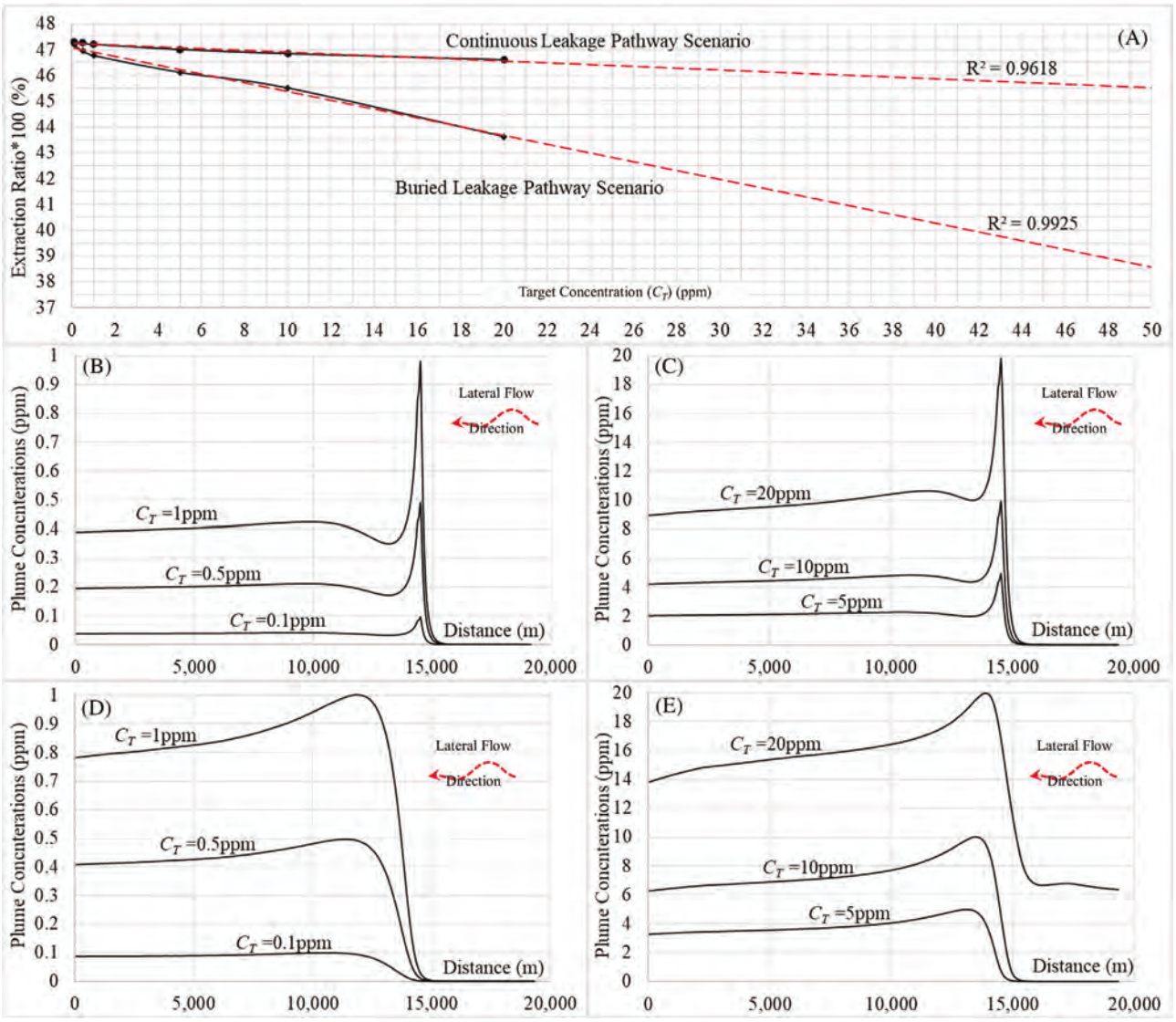

Figure 7. (A) The sensitivity of the extraction ratios to the change in the target concentrations. (B–E) The concentration profiles of the plume along the interface between Kern River and Etchegoin formations (marked by a red line in Fig. 6A) for different target concentration scenario under the leakage mechanisms of (B, C) continuous or (D, E) buried pathway.

results if the control of migrating fluids also included the fate of injected CO_2. Moreover, a transient multiphase model is needed to determine how long the extraction well should be operating to control the leakage after ceasing the CO_2 injection.

Discussion

The study findings showed that designing an optimal extraction scheme to control the potential brine leakage from CO_2 storage formations is not a trivial problem as it includes large-sized and complex solution spaces. A global optimizer is necessary to be incorporated in this problem to deal with such non-convex, multivariant, and discontinuous solution spaces. The GA was successfully employed in this study to find the most optimal extraction control system for experimental and numerical leakage problems. The GA results elucidated that the permeability architecture of the storage zone can highly alter the optimal extraction location, while the fracture permeabilities can have more impact on the extraction rates. It was also found that errors in well placements or the used pumping rates during operation can lead to a leakage plume that violates the maximum allowed concentrations in the shallow aquifer (e.g., MLCs or NITVs). These findings suggest that the

extraction well locations can be determined prior to CO_2 injection using high-resolution data on storage zone heterogeneity collected during site investigation. Such high-resolution data can be obtained by applying techniques like cross-well seismic imaging between the injection and monitoring wells before operation.[114,115] However, the extraction rates can be initially estimated using the available data prior to CO_2 injection, but such rates would need to be revisited and adjusted based on the leakage pathways' permeabilities. Such permeabilities can be inferred using transient monitoring data on the pressure changes and plume development in the system that become available after GCS operation and leakage onset.

The lack of accurate knowledge about deep geological settings and its transport properties in GCS sites (e.g., storage zone heterogeneity and dispersivity) is typically addressed through considering different realizations of the expected system characteristics for modeling the leakage.[116–118] Moreover, caprock damage zones may not even exist at the time of designing the extraction wells, which requires developing more realizations to represent all possible permeabilities of the potential leakage pathways and simulate all likely distributions of the plume. Dealing with all these realizations under the same optimization problem can be challenging. Aitokhuehi and Durlofsky,[119] Van Essen et al.,[120] and Wang et al.[121] introduced various approaches to integrate multiple system realizations under a single optimization problem and find the overall optimal solution. However, under such conditions the optimization process can be computationally intensive. In this context, the experimental analysis of this study showed that uncertainty in specific system properties may not affect the extraction system design in some cases at least the ones studied here. Such finding indicates the ability to reduce the size of the parameter-space that need to be sampled to develop the system realizations, which will decrease the required computational capacity for the optimization process. This reduction in the parameter ensemble size can be obtained by filtering the parameters based on their sensitivities to target predictions (i.e., plume concentration in the shallow aquifer) using some tool like PESTPP-SEN.[122] However, the approach was also validated to be used stochastically under extreme uncertainty conditions in case the parameter-ensemble reduction was not valid.

The performed numerical experiments in this study showed an inverse relationship between the target concentrations in the shallow aquifer and the required extraction rates from the deep storage zone to control the leakage plume, particularly in the case of leakage from a buried pathway or a caprock fracture. This suggests the possibility of reducing the necessary extraction rate of the control system if the estimated NITVs for the site of interest were higher than the MCLs and regulators decided to use them. Such a decision should also consider the native quality of the brine prior migration and the expected geochemical reactions along its travel distance to the shallow aquifer. It should also be noted that GCS technology is still in its infancy, but in the future, like many mining projects, GCS operators will be allowed to apply for alternate concentration limits (ACLs) at the point of exposure (i.e., shallow aquifer) if groundwater is not usable and neglectable human-health impact and low ecological exposure level are proven.[123,124]

Applying an integrated control system is another approach to reduce the required extraction rates to control the leakage plume. In this system, the deep extraction wells are responsible for alleviating the plume concentrations at the shallow aquifer to a certain level that can be further managed by shallow remediation methods. By that, the operational cost of the control process can be reasonably decreased.

Conclusions

Pressure build-up in the storage formation due to the injection of CO_2 for geological sequestration, risks caprock integrity and can cause upward leakage of the formation brine. Different researchers have proposed brine extraction as a pressure management technique to reduce the geomechanical risks of damaging the caprock. In this study, we introduce the use of the same technique as an emergency remediation strategy to control the potential brine leakage from CO_2 storage formations when it occurs. Handling large amounts of extracted brine can be technically challenging and costly. Thus, we incorporated the GA with FEFLOW-based transport model to find the optimum locations and minimum pumping rates of the extraction wells. An intermediate-scale leakage control experiment was conducted in an ~8m long soil tank to validate the applicability of the developed approach. In this experiment, the leakage plume was controlled by an extraction well located in the storage zone so that the plume concentrations at the shallow aquifer do not exceed predefined limits (zero ppm in this case).

Moreover, we examined the practicality of the leakage control technique to be applied in the field under a realistic scale of the leakage problem using numerical simulations. For this analysis, a hypothetical leakage event from the Pond fault in the Vedder formation of San Joaquin Basin was controlled using a single extraction well designed based on the results of the GA.

The conclusions based on the conducted experimental and numerical analysis in this study are:

1. Finding the optimal extraction location and rate to control a brine leakage plume is not a trivial problem as it includes large-sized, nonconvex solution space.
2. The GA was able to deal with such solution space and find the optimal well locations and pumping rates for the tested experimental and numerical leakage problems.
3. Accurate mapping of the storage zone heterogeneity and reasonable predictions of the future fracture permeabilities are required for designing the leakage control system as both parameters can significantly affect the optimal locations and pumping rates of the extraction wells.
4. By implementing the selected extraction well and pumping rate in the soil tank, the leakage flow was reversed to the storage formations and the plume dispersion was maintained at close proximity to the caprock fractures.
5. The tested extraction system in the tank was able to control the leakage plume even after a pump failure that lasted for 3.5 h during a leakage event that continued for ∼317 h.
6. The proposed design approach was successfully tested and implemented in a stochastic framework to address the possibility of having highly uncertain field data.
7. The numerical experiments showed that by extracting brine volumes less than half of the injected amount of CO_2 in the Vedder formation, the plume concentrations at the shallow aquifer mass were maintained below a concentration of 0.1 ppm; such results indicate the practicality of using the extraction technique for brine leakage control.
8. An inverse relationship was found between the leakage target concentrations in the shallow aquifer and the extraction rates from the storage formation; this relation can be used to reduce the control system cost by allowing for higher contaminant concentration in the shallow aquifer if this was acceptable by authorities.
9. This inverse relationship was more pronounced when a leakage through a buried pathway or a caprock fracture was controlled compared to a continuous leakage pathway mechanism due to the efficient utilization of the dilution capacity of the overlying formations in the former scenarios.
10. The EPA requirement of developing an emergency remedial response strategy will be satisfied by designing a leakage control system using the tested approach in this study; such system will be initially utilized for pressure build-up management, until a leakage event happens, only then, it will be used as an emergency response tool for leakage control.

The authors would like to emphasize that the basic challenge in working with the problem of deep geologic storage is the unavailability of field data to test or validate methods. Considering this critical limitation, we have presented an approach to validate and test a modified method after the one presented by the modeling group at Lawrence Berkeley National Laboratory, with whom we have collaborated in the past, so that the method can be used for both preleakage pressure management and postleakage plume migration control. We believe that in the absence of filed data, the use of intermediate-scale testing to validate this method is novel. To our knowledge, based on an extensive literature review, we are not aware of any other work where such testing approach has been adapted. The significance of the present study contribution comes from the practical value of the findings in the context of showing that optimal extraction systems can be designed to protect shallow groundwater in case of a leakage.

The authors admit that the interpretation of the experimental results in this study cannot be directly comparable to field-scale leakage problems. However, the examination of the applicability of the method in this study would never be possible except via adapting the technique of intermediate-scale testing. This testing method offered an opportunity to evaluate the optimization approach under full control of the uncertainties in the system. Therefore, the experimental work of this study provided an initial validation of the optimization method applicability to be used for designing the extraction wells and the efficiency of these wells in controlling the potential

brine leakage from CO_2 repositories. Such validation was further supported by field-scale numerical experiments to verify the experimental results and explore how practical the extraction technique is while controlling a large-scale leakage event.

Acknowledgements

The authors gratefully acknowledge funding from the NSF Hydrologic Sciences Program Award 1702060 for supporting this research project. Authors would like to express appreciation to DHI, USA for supporting this research by offering an academic license of FEFLOW. We thank all laboratory colleges and undergraduate students who helped in the experimental work: Cody Goebel, and Analise Butler. Dr Andrew Trautz from the Engineer Research and Development Center of the Army Corps of Engineers contributed to the design and development of the experimental test system. His contributions and guidance during the early stages of the experimental plan are gratefully acknowledged. We also acknowledge the contributions of Dr Ye Zhang, the PI of the collaborative project at the University of Wyoming. The authors would like to express their extreme gratitude for the constructive discussions with Dr Abdullah Cihan, Staff Scientist at Lawrence Berkeley National Laboratory, that helped to set the fundamentals and scientific bases of this study. A sincere "thank you" goes to Sarah Awara for her diligent proofreading of this paper. Raw data generated during the experiment of the present study are publicly available and stored in the HydroShare digital repositorhttps://doi.org/10.4211/hs.ea5d0091789043e8a8091ae43d314554.

References

1. Bachu S. Screening and ranking of sedimentary basins for sequestration of CO2 in geological media in response to climate change. Environ Geol. 2003;44(3):277–89.
2. IPCC IPCC Special. Report on carbon dioxide capture and storage. Prepared by working group III of the intergovernmental panel on climate change. Cambridge, UK: IPCC; 2005. p. 442.
3. Lackner KS. A guide to CO_2 sequestration. Science. 2003;300(5626):1677–8.
4. U.S. DOE. Carbon sequestration atlas of the United States and Canada. Fifth Edition. Washington, DC: Department of Energy/NETL; 2015. p. 24.
5. Celia MA, Nordbotten JM, Court B, Dobossy M, Bachu S. Field-scale application of a semi-analytical model for estimation of CO_2 and brine leakage along old wells. Int J Greenhouse Gas Control. 2011;5(2):257–69.
6. Gasda SE, Bachu S, Celia MA. Spatial characterization of the location of potentially leaky wells penetrating a geological formation in a mature sedimentary basin. Environ Geol. 2004;46(6-7):707–20.
7. Rutqvist J, Birkholzer J, Cappa F, Tsang CF. Estimating maximum sustainable injection pressure during geological sequestration of CO_2 using coupled fluid flow and geomechanical fault-slip analysis. Energy Convers Manage. 2007;48(6):1798–807.
8. Rutqvist J, Birkholzer JT, Tsang CF. Coupled reservoir–geomechanical analysis of the potential for tensile and shear failure associated with CO_2 injection in multilayered reservoir–caprock systems. Int J Rock Mech Min Sci. 2008;45(2):132–43.
9. Birkholzer J, Zhou Q, Tsang C. Large-scale impact of CO_2 storage in deep saline aquifers: A sensitivity study on pressure response in stratified systems. Int J Greenhouse Gas Control. 2009;3(2):181–94.
10. Oldenburg CM, Cihan A, Zhou Q, Fairweather S, Spangler LH. Geologic carbon sequestration injection wells in overpressured storage reservoirs: estimating area of review. Greenhouse Gases: Sci Technol. 2016;6(6):775–86.
11. Bergmo PES, Grimstad AA, Lindeberg E. Simultaneous CO_2 injection and water production to optimise aquifer storage capacity. Int J Greenhouse Gas Control. 2011;5(3):555–64.
12. Birkholzer JT, Cihan A, Zhou Q. Impact-driven pressure management via targeted brine extraction—conceptual studies of CO_2 storage in saline formations. Int J Greenhouse Gas Control. 2012;7:168–80.
13. Buscheck TA, Sun Y, Hao Y, Wolery TJ, Bourcier W, Tompson AFB, et al. Combining brine extraction, desalination, and residual-brine reinjection with CO_2 storage in saline formations: Implications for pressure management, capacity, and risk mitigation. Energy Procedia. 2011;4:4283–90.
14. Buscheck TA, White JA, Chen M, Sun Y, Hao Y, Aines RD, et al. Pre-injection brine production for managing pressure in compartmentalized CO_2 storage reservoirs. Energy Procedia. 2014;63:5333–40.
15. Birkholzer JT, Zhou Q. Basin-scale hydrogeologic impacts of CO_2 storage: capacity and regulatory implications. Int J Greenhouse Gas Control. 2009;3(6):745–56.
16. Cameron DA, Durlofsky LJ. Optimization of well placement, CO_2 injection rates, and brine cycling for geological carbon sequestration. Int J Greenhouse Gas Control. 2012;10:100–12.
17. Court B, Bandilla KW, Celia MA, Buscheck TA, Martin J, Dobossy M, et al. Initial evaluation of advantageous synergies associated with simultaneous brine production and CO_2 geological sequestration. Int J Greenhouse Gas Control. 2012;8:90–100.
18. Sullivan EJ, Chu S, Stauffer PH, Middleton RS, Pawar RJ. A method and cost model for treatment of water extracted during geologic CO_2 storage. Int J Greenhouse Gas Control. 2013;12:372–81.
19. Cihan A, Birkholzer JT, Bianchi M. Optimal well placement and brine extraction for pressure management during CO_2 sequestration. Int J Greenhouse Gas Control. 2015;42:175–87.
20. González-Nicolás A, Cihan A, Petrusak R, Zhou Q, Trautz R, Riestenberg D, et al. Pressure management via brine extraction in geological CO_2 storage: adaptive optimization

strategies under poorly characterized reservoir conditions. Int J Greenhouse Gas Control. 2019;83:176–85.
21. Detwiler RL, Morris JP. Fracture initiation, propagation, and permeability evolution. In: Stéphanie Vialle J. A. a. J. W. C., editors. Geological carbon storage: subsurface seals and caprock integrity, geophysical monograph. s.l. Hoboken, NJ: John Wiley and Sons; 2019. pp. 121–35.
22. Lei Q, Latham JP, Tsang CF. The use of discrete fracture networks for modelling coupled geomechanical and hydrological behaviour of fractured rocks. Comput Geotech. 2017;85:151–76.
23. Court B. Safety and water challenges in CCS: modeling studies to quantify CO_2 and brine leakage risk and evaluate promising synergies for active and integrated water management. Ph.D. Dissertation. Princeton, NJ: Princeton University; 2011.
24. EPA US. 40 CFR Parts 124, 144, 145, 146, and 147 Federal requirements under the underground injection (UIC) program for carbon dioxide (CO_2) geologic sequestration (GS) wells; Final Rule, [EPA–HQ–OW–2008–0390 FRL–9232–7], RIN 2040–AE98, s.l.: Environmental Protection Agency. 2010: 77230–303.
25. Siirila ER, Navarre-Sitchler AK, Maxwell RM, McCray JE. A quantitative methodology to assess the risks to human health from CO_2 leakage into groundwater. Adv Water Res. 2012;36:146–64.
26. Last G, Murray C, Bott Y, Brown C. Threshold values for identification of contamination predicted by reduced-order models. Energy Procedia. 2014;63:3589–97.
27. Carroll S, Keating E, Mansoor K, Dai Z, Sun Y, Trainor-Guitton W, et al. Key factors for determining groundwater impacts due to leakage from geologic carbon sequestration reservoirs. Int J Greenhouse Gas Control. 2014;29:153–68.
28. Keating E, Bacon D, Carroll S, Mansoor K, Sun Y, Zheng L, et al. Applicability of aquifer impact models to support decisions at CO_2 sequestration sites. Int J Greenhouse Gas Control. 2016;52:319–30.
29. Mansoor K, Carroll S, Sun Y. The role of wellbore remediation on the evolution of groundwater quality from CO_2 and brine leakage. Energy Procedia. 2014;63:4799–806.
30. Pawar R, Bromhal GS, Chu S, Dilmore RM, Oldenburg CM, Stauffer PH, et al. The national risk assessment partnership's integrated assessment model for carbon storage: a tool to support decision making amidst uncertainty. Int J Greenhouse Gas Control. 2016;52:175–89.
31. Qafoku NP, Lawter AR, Bacon DH, Zheng L, Kylea J, Browna CF, et al. Review of the impacts of leaking CO_2 gas and brine on groundwater quality. Earth Sci Rev. 2017;169:69–84.
32. Xiao T, McPherson B, Esser R, Jia W, Dai Z, Chu S. Chemical impacts of potential CO_2 and brine leakage on groundwater quality with quantitative risk assessment: A case study of the Farnsworth Unit. Energies. 2020;13(24):6574.
33. Xiao T, McPherson B, Pana F, Esser R, Jia W, Bordelon A, et al. Potential chemical impacts of CO_2 leakage on underground source of drinking water assessed by quantitative risk analysis. Int J Greenhouse Gas Control. 2016;50:305–16.
34. Yang Y, Dilmore R, Bromhal G, Small M. Toward an adaptive monitoring design for leakage risk–closing the loop of monitoring and modeling. Int J Greenhouse Gas Control. 2018;76:125–41.
35. Yang Y, Dilmore RM, Mansoor K, Buscheck TA, Bromhala GS. Integration of wellbore pressure measurement and groundwater quality monitoring to enhance detectability of brine and CO_2 leakage. Int J Greenhouse Gas Control. 2019;85:143–55.
36. Ahlfeld DP, Heidari M. Applications of optimal hydraulic control to ground-water systems. J Water Resour Plann Manage. 1994;120(3):350–65.
37. Mantoglou A, Papantoniou M, Giannoulopoulos P. Management of coastal aquifers based on nonlinear optimization and evolutionary algorithms. J Hydrol. 2004;297(1-4):209–28.
38. Zhang Z, Agarwal RK. Numerical simulation and optimization of CO_2 sequestration in saline aquifers for vertical and horizontal well injection. Comput Geosci. 2012;16(4): 891–9.
39. Liu D, Agarwal R, Li Y. Numerical simulation and optimization of CO_2 -enhanced water recovery by employing a genetic algorithm. J Cleaner Prod. 2016;133:994–1007.
40. Pruess K. TOUGH2: A general-purpose numerical simulator for multiphase nonisothermal flows. 1991, https://doi.org/10.2172/138333.
41. Liu S, Agarwal R, Sun B, Wang B, Lia H, Xu J, et al. Numerical simulation and optimization of injection rates and wells placement for carbon dioxide enhanced gas recovery using a genetic algorithm. J Cleaner Prod. 2020;280:124512.
42. Bangerth W, Klie H, Wheeler MF, Stoffa PL, Sen MK. On optimization algorithms for the reservoir oil well placement problem. Comput Geosci. 2006;10(3):303–19.
43. Janiga D, Czarnota R, Stopa J, Wojnarowski P. Self-adapt reservoir clusterization method to enhance robustness of well placement optimization. J Pet Sci Eng. 2019a;173:37–52.
44. Janiga D, Czarnota R, Stopa J, Wojnarowski P, Kosowski P. Utilization of nature-inspired algorithms for gas condensate reservoir optimization. Soft Computing. 2019b;23(14):5619–31.
45. Diersch GHJ. FEFLOW: finite element modeling of flow, mass and heat transport in porous and fractured media. Heidelberg, Germany: Springer Science and Business Media; 2014. Volume 10. pp. 978-3.
46. Walker WE, Harremoës P, Rotmans J, van der Sluijs JP, van Asselt MBA, Janssen P, et al. Defining uncertainty: a conceptual basis for uncertainty management in model-based decision support. Integr Assess. 2003;4(1):5–17.
47. Askar AH, Illangasekare TH, Trautz A, Solovský J, Zhang Y, Fučík R. Exploring the impacts of source condition uncertainties on far-field brine leakage plume predictions in geologic storage of CO_2: integrating intermediate-scale laboratory testing with numerical modeling. Water Resour Res. 2021a;57(9):e2021WR029679.
48. Birkholzer JT, Zhou Q, Cortis A, Finsterle S. A sensitivity study on regional pressure buildup from large-scale CO_2 storage projects. Energy Procedia. 2011;4:4371–8.
49. Wainwright HM, Finsterle S, Zhou Q, Birkholzer JT. Modeling the performance of large-scale CO_2 storage systems: a comparison of different sensitivity analysis methods. Int J Greenhouse Gas Control. 2013;17:189–205.
50. Zhou Q, Birkholzer J. On scale and magnitude of pressure build-up induced by large-scale geologic storage of CO_2. Greenhouse Gases: Sci Technol. 2011;1(1):11–20.

51. Deep K, Singh KP, Kansal ML, Mohan C. A real coded genetic algorithm for solving integer and mixed integer optimization problems. Appl Math Comput. 2009;212(2):505–18.
52. MathWorks. Global optimization toolbox: user's guide. Natick, MA: The MathWorks; 2020.
53. Deb K. An efficient constraint handling method for genetic algorithms. Comput Meth Appl Mech Eng. 2000;186:311–38.
54. Askar AH, Illangasekare TH, Carmen IAM. Monitoring brine leakage from deep geologic formations storing carbon dioxide: design framework validation using intermediate-scale experiment. Water Resour Res. 2021;57(12). https://doi.org/10.1029/2021WR031005
55. White J, Knowling MJ, Fienen MN, Siade A, Rea O, Martinez G. A model-independent tool for evolutionary constrained multi-objective optimization under uncertainty. Environ Model Software. 2022;149:105316.
56. Saad S, Javadi A, Chugh T, Farmani R. Optimal management of mixed hydraulic barriers in coastal aquifers using multi-objective Bayesian optimization. J Hydrol. 2022;612:128021.
57. Neuman SP. Universal scaling of hydraulic conductivities and dispersivities in geologic media. Water Resour Res. 1990;26(8):1749–58.
58. Doherty J. Calibration and uncertainty analysis for complex environmental models. In: Watermark numerical computing. 1st ed., Brisbane, Australia: Watermark Numerical Computing; 2015.
59. Doherty JE, Hunt RJ, Tonkin MJ. Approaches to highly parameterized inversion: A guide to using PEST for model-parameter and predictive-uncertainty analysis. US Geological Survey Scientific Investigations Report. 2010;2010–5211.
60. Feng J, Li L, Jin J, Dai J, Luo P. An improved geomechanical model for the prediction of fracture generation and distribution in brittle reservoirs. PloS one. 2018;13(11):e0205958 (1:28).
61. Ingram GM,d Urai JL. Top-seal leakage through faults and fractures: the role of Mudrock properties. Geol Soc Lond Special Publ. 1999;158(1):125–35.
62. Krawczyk CM, Tanner DC, Henk A, Trappe H. Seismic and sub-seismic deformation prediction in the context of geological carbon trapping and storage. In: Liebscher A & Münch U, editors. Geological storage of CO_2–long term security aspects. Cham, Switzerland: Springer; 2015. pp. 97–113.
63. Ligtenberg JH. Detection of fluid migration pathways in seismic data: implications for fault seal analysis. Basin Res. 2005;17(1):141–53.
64. Lohr T, Krawczyk CM, Tanner DC, Samiee R. Prediction of sub-seismic faults and fractures-integration of 3D seismic data, 3D retrodeformation, and well data on an example of deformation around an inverted fault. AAPG Bull. 2008;92(4):473–85.
65. Ziesch J, Tanner DC, Krawczyk CM. Subseismic pathway prediction by three-dimensional structural restoration and strain analysis based on seismic interpretation. AAPG Bull. 2019;103(10):2317–42.
66. Vialle S, Druhan JL, Maher K. Multi-phase flow simulation of CO_2 leakage through a fractured caprock in response to mitigation strategies. Int J Greenhouse Gas Control. 2016;44:11–25.
67. Deutsch CV. A sequential indicator simulation program for categorical variables with point and block data: BlockSIS.Comput Geosci. 2006;32(10):1669–81.
68. Remy N, Boucher A, Wu J. Applied geostatistics with SGeMS: a user's guide. New York: Cambridge University Press; 2009.
69. Hermanrud C, Andresen T, Eiken O, Hansen H, Janbu A, Lippard J, et al. Storage of CO_2 in saline aquifers–lessons learned from 10 years of injection into the Utsira formation in the Sleipner area. Energy Procedia. 2009;1(1):1997-2004.
70. Torp TA, Gale J. Demonstrating storage of CO_2 in geological reservoirs: the Sleipner and SACS projects. Energy. 2004;29(9-10):1361-9.
71. Zweigel P, Arts R, Lothe AE, Lindeberg EB. Reservoir geology of the Utsira Formation at the first industrial-scale underground CO_2 storage site (Sleipner area, North Sea). Geological Society, London, Special Publications. 2004;233(1):165-80.
72. USGS. Petroleum systems and geologic assessment of oil and gas in the SanJoaquin Basin province. In: Scheirer AH, editor, Professional paper1713, Los Angeles, CA: U.S. Geological Survey. 2007.
73. Birkholzer JT, Nicot JP, Oldenburg CM, Zhou Q, Kraemer S, Bandilla K. Brine flow up a well caused by pressure perturbation from geologic carbon sequestration: Static and dynamic evaluations. Int J Greenhouse Gas Control. 2011;5(4):850–61.
74. Jeanne P, Rutqvist J, Foxall W, Rinaldi AP, Wainwright HM, Zhou Q, et al. Effects of the distribution and evolution of the coefficient of friction along a fault on the assessment of the seismic ctivity associated with a hypothetical industrial-scale geologic CO_2 sequestration operation. Int J Greenhouse Gas Control. 2017;66:254–63.
75. Oldenburg CM, Jordan PD, Burton E. Recommendations for geologic carbon sequestration in California: I. Siting criteria and monitoring approaches, II. example application case study. Final report deliverable under ARB agreement No. 15ISD007, Berkeley, CA, Energy Geosciences Division - Lawrence Berkeley National Laboratory; 2017.
76. Downey C, Clinkenbeard J. An overview of geologic carbon sequestration potential in California. Sacramento, CA: California Energy Commission USDOE; 2005. https://doi.org/10.2172/903323
77. Pawar R, Bromhal G, Carroll S, Chu S, Dilmore R, Gastelum J, et al. Quantification of key long-term risks at CO_2 sequestration sites: latest results from US DOE's national risk assessment partnership (NRAP) project. Energy Procedia. 2014;63:4816–23.
78. EPA.Federal Requirements Under the Underground Injection Control (UIC) Program for Carbon Dioxide (CO2) Geologic Sequestration (GS) Wells, Final Rule. Federal Register, 40 CFR Parts 124, 144, 145. EPA; 2010.
79. Jeanne P, Haruko J, Wainwright M, Foxall W, Bachmann C, Zhou Q, et al. Effects of in situ stress measurement uncertainties on assessment of predicted seismic activity and risk associated with a hypothetical industrial-scale geologic CO_2 sequestration operation. J Rock Mech Geotech Eng. 2016;8(6):873–85.

80. Gassiat C, Gleeson T, Lefebvre R, McKenzie J. Hydraulic fracturing in faulted sedimentary basins: numerical simulation of potential contamination of shallow aquifers over long time scales. Water Resour Res. 2013;49(12):8310–27.
81. Zoback MD, Gorelick SM. Earthquake triggering and large-scale geologic storage of carbon dioxide. Proc Natl Acad Sci. 2012;109(26):10164–8.
82. Jeanne P, Guglielmi Y, Rutqvist J, Nussbaum C, Birkholzer J. Permeability variations associated with fault reactivation in a claystone formation investigated by field experiments and numerical simulations. J Geophys Res: Solid Earth. 2018;123(2):1694–710.
83. Guglielmi Y, Elsworth D, Cappa F, Henry P, Gout C, Dick P, et al. In situ observations on the coupling between hydraulic diffusivity and displacements during fault reactivation in shales. J Geophys Res: Solid Earth. 2015;120(11): 7729–48.
84. Cappa F, Guglielmi Y, Nussbaum C, Birkholzer J. On the relationship between fault permeability increases, induced stress perturbation, and the growth of aseismic slip during fluid injection. Geophys Res Lett. 2018;45(20):11–012.
85. Rutqvist J, Graupner B, Guglielmi Y, Kim T, Maßmann J, Nguyen TS, et al. An international model comparison study of controlled fault activation experiments in argillaceous claystone at the Mont Terri Laboratory. Int J Rock Mech Min Sci. 2020;136:104505.
86. Park JW, Guglielmi Y, Graupner B, Rutqvist J, Kim T, Park E-S. Modeling of fluid injection-induced fault reactivation using coupled fluid flow and mechanical interface model. Int J Rock Mech Min Sci. 2020;132:104373.
87. Palladino G, Alsop GI, Grippa A, Zvirtes G, Phillip RP, Hursta A. Sandstone-filled normal faults: a case study from central, California. J Struct Geol. 2018;110:86–101.
88. Guglielmi Y, Nussbaum C, Cappac F, De Barros L, Rutqvist J, Birkholzera J. Field-scale fault reactivation experiments by fluid injection highlight aseismic leakage in caprock analogs: Implications for CO_2 sequestration. Int J Greenhouse Gas Control. 2021;111:103471.
89. Shapiro SA. Fluid-induced seismicity. 1st ed. Cambridge, UK: Cambridge University Press; 2018.
90. Boston B, Moore GF, Jurado MJ, Sone H. Deformation of the Nankai Trough inner accretionary prism: The role of inherited structures. Geochem Geophys Geosyst. 2016;17(2): 485–500.
91. Celia MA, Nordbotten JM. Practical modeling approaches for geological storage of carbon dioxide. Groundwater. 2009;47(5):627–38.
92. Jeanne P, Guglielmi Y, Cappa F. Dissimilar properties within a carbonate-reservoir's small fault zone, and their impact on the pressurization and leakage associated with CO_2 injection. J Struct Geol. 2013;47:25–35.
93. Huang ZQ, Winterfeld PH, Xiong Y, Wu Y-S, Yao J. Parallel simulation of fully-coupled thermal-hydro-mechanical processes in CO2 leakage through fluid-driven fracture zones. Int J Greenhouse Gas Control. 2015;34:39–51.
94. Cihan A, Birkholzer JT, Zhou Q. Pressure buildup and brine migration during CO_2 storage in multilayered aquifers. Groundwater. 2013;51(2):252–67.
95. Bandilla KW, Celia MA, Birkholzer JT, Cihan A, Leister EC. Multiphase modeling of geologic carbon sequestration in saline aquifers. Groundwater. 2015;53(3):362–77.
96. Nicot JP. Evaluation of large-scale CO_2 storage on fresh-water sections of aquifers: An example from the Texas Gulf Coast Basin. Int J Greenhouse Gas Control. 2008;2(4):582–93.
97. Zhou Q, Birkholzer JT, Tsang C. A semi-analytical solution for large-scale injection-induced pressure perturbation and leakage in a laterally bounded aquifer–aquitard system. Transp Porous Media. 2009;78(1):127–48.
98. Deming D. Introduction to hydrogeology. 1st ed. s.l.:McGraw-Hill Science, Engineering and Mathematics, 2001.
99. Osborne MJ, Swarbrick RE. Mechanisms for generating overpressure in sedimentary basins: A reevaluation. AAPG Bull. 1997;81(6):1023–41.
100. Gelhar LW, Welty C, Rehfeldt KR. A critical review of data on field-scale dispersion in aquifers. Water Resour Res. 1992;28(7):1955–74.
101. Fossen H, Schultz RA, Shipton ZK, Mair K. Deformation bands in sandstone: a review. J Geol Soc. 2007;164(4):755–69.
102. Tondi E. Nucleation, development and petrophysical properties of faults in carbonate grainstones: evidence from the San Vito Lo Capo peninsula (Sicily, Italy). J Struct Geol. 2007;29(4):614–28.
103. Tondi E, Antonellini M, Aydin A, Marchegiani L, Cello G. The role of deformation bands, stylolites and sheared stylolites in fault development in carbonate grainstones of Majella Mountain, Italy. J Struct Geol. 2006;28(3):376–91.
104. Wagoner J. 3D geologic modeling of the southern San Joaquin basin for the Westcarb Kimberlina demonstration project-A status report (No. LLNL-TR-410813), Livermore, CA: Lawrence Livermore National Lab; 2009.
105. Wunsch A, Navarre-Sitchler AK, McCray JE. Geochemical implications of brine leakage into freshwater aquifers. Groundwater. 2013;51(6):855–65.
106. Zheng L, Carroll S, Bianchi M, Mansoor K, Sun Y, Birkholzer J. Reduced order models for prediction of groundwater quality imp for prediction of groundwater quality impacts from CO_2 and brine leakage. Energy Procedia. 2014;63(C):4875–83.
107. Ford EP, Moeinikia F, Lohne HP, Arild Ø, Majoumerd MM, Fjelde KK. Leakage calculator for plugged and abandoned wells. In SPE Bergen One Day Seminar. Bergen, Norway; 2017. https://doi.org/10.2118/185890-MS
108. Harp DR, Pawar R, Carey JW, Gable CW. Reduced order models of transient CO_2 and brine leakage along abandoned wellbores from geologic carbon sequestration reservoirs. Int J Greenhouse Gas Control. 2016;45:150-62.
109. Humez P, Audigane P, Lions J, Chiaberge C, Bellenfant G. Modeling of CO_2 leakage up through an abandoned well from deep saline aquifer to shallow fresh groundwaters. Transp Porous Media. 2011;90(1):153-81.
110. Nordbotten JM, Kavetski D, Celia MA, Bachu S. Model for CO_2 leakage including multiple geological layers and multiple leaky wells. Environ Sci Technol. 2009;43(3): 743-9.
111. Tao Q, Checkai DA, Huerta NJ, Bryant SL. Estimating CO_2 fluxes along leaky wellbores. Spe J. 2014;19(02):227-38.
112. Tao Q, Bryant SL Well permeability estimation and CO_2 leakage rates. Int J Greenhouse Gas Control. 2014;22: 77-87.

113. Yu B, Wang L, Liu Y. Optimization of injection location based on simulations of CO_2 leakage through multiple leakage pathways. Asia-Pac J Chem Eng. 2016;11(4):620-9.
114. Nalonnil A, Marion B. High-resolution reservoir monitoring using crosswell seismic. SPE Reserv Eval Eng. 2012;15(01):25–30.
115. Yu G, Marion B, Bryans B, Carrillo P, Guo W, Pang Y, et al. Crosswell seismic imaging for deep gas reservoir characterization. Geophysics. 2008;73(6):B117-26.
116. Chen B, Harp DR, Lin Y, Keating EH, Pawar RJ. Geologic CO_2 sequestration monitoring design: A machine learning and uncertainty quantification-based approach. Appl Energy. 2018;225:332–45.
117. Jeong J, Park E, Han WS, Kim K-Y, Yund S-T. Feasibility study to optimize a near-surface sensor network design for improving detectability of CO_2 leakage at a geologic storage site. J Hydrol. 2019;572:32–39.
118. Yonkofski CM, Gastelum JA, Porter EA, Rodriguez LR, Bacon DH, Brown CF. An optimization approach to design monitoring schemes for CO_2 leakage detection. Int J Greenhouse Gas Control. 2016;47:233–9.
119. Aitokhuehi I, Durlofsky LJ. Optimizing the performance of smart wells in complex reservoirs using continuously updated geological models. J Pet Sci Eng. 2005;48(3-4):254–64.
120. Van Essen G, Zandvliet MJ, Van den Hof PMJ, Bosgra OH, Jansen JD. Robust waterflooding optimization of multiple geological scenarios. SPE J. 2009;14(1):202–10.
121. Wang H, Ciaurri DE, Durlofsky LJ, Cominelli A. Optimal well placement under uncertainty using a retrospective optimization framework. SPE J. 2012;17(1):112–21.
122. White JT, Hunt RJ, Fienen MN, Doherty JE. Approaches to highly parameterized inversion: PEST++ Version 5, a software suite for parameter estimation, uncertainty analysis, management optimization and sensitivity analysis (No. 7-C26). US Geological Survey. 2020.
123. U.S. EPA. Alternate Concentration limit guidance Part 1: ACL policy and information requirements. 1987;40:CFR §264.94(a)(3), Washington, DC: U.S. Environmental Protection Agency.
124. U.S. EPA. Alternate concentration limit guidance Part 2: case studies. Washington, DC: U.S. Environmental Protection Agency. 1988;40: CFR §264.94(b).

Ahmad Askar

Ahmad Askar is a hydrogeologist/senior groundwater modeler at INTERA Inc. His consulting work focuses on developing sustainable groundwater resources and mitigating the environmental risks of mining projects through exploring the potential uncertainty in model predictions related to the efficacy of remediation strategies. His scientific emphasis centers on exploring new methods for better management of deep brine leakage from CO_2 geological storages. He earned his PhD in Civil and Environmental Engineering from Colorado School of Mines.

Tissa Illangasekare

Tissa Illangasekare is the AMAX Distinguished Chair and the director of the Center for Experimental Study of Subsurface Environmental Processes at CSM. He is a Fellow of AGU, AAAS, ASCE, SSSA, and Sri Lanka National Academy of Sciences and a foreign member of the Academy of Europe. Recipient EGU's Darcy Medal, AGU's Langbein Lecture Award, and 7th Prince Sultan Bin Abdulaziz International Groundwater Prize. He was the past editor of *Water Resources Research* and the current editor of *AGU Advances* and *AGU Perspectives of Earth and Planetary Scientists*. He is the chief section editor of *Frontiers in Water and Human Health*. His research is in numerical and physical modeling of porous media processes.